Eur. J. Mineral.
2010, **22**, 577–594
Published online May 2010

Hydrothermal origin of manganese in the high-pressure ophiolite metasediments of Praborna ore deposit (Aosta Valley, Western Alps)

SIMONE TUMIATI[1,*], SILVANA MARTIN[2] and GASTON GODARD[3]

[1] Dipartimento di Scienze della Terra ''Ardito Desio'', Università degli Studi di Milano, via Botticelli 23, 20133 Milano, Italy
*Corresponding author, e-mail: simone.tumiati@unimi.it
[2] Dipartimento di Geoscienze, Università degli Studi di Padova, via Giotto 1, 35137 Padova, Italy
[3] Equipe Géobiosphère actuelle et primitive; Institut de Physique du Globe de Paris, Université Paris-Diderot, CNRS, 2 place, Jussieu, 75005 Paris, France

Abstract: The manganese ore deposit of Praborna crops out in the Zermatt-Saas unit of the Western Alps, in the St. Marcel valley. It represents a Jurassic ophiolitic sedimentary cover subducted at high-pressure conditions during the Alpine orogeny. Major- and trace-element analyses of representative samples of the ore and the host metasediments were collected to geochemically characterise the deposit. Selected phases (piemontite, braunite, garnet, clinopyroxene, white mica and manganiandrosite) were investigated with ion and electron microprobes to link the mineral chemistry to the bulk-rock chemistry. Compared to shales, Praborna is enriched in Mn (up to 38.7 wt% Mn_2O_3) and in many trace elements (Sc, Co, Ni, Cu, Ge, As, Sr, Ag, Sb, Te, Ba, Tl, Pb and Bi). The bulk-rock REE pattern suggests 20 % hydrogenous and 80 % hydrothermal inputs in the proto-ore. Compared to the shale, the hanging-wall Mn-poor schists share with the Mn ore body the enrichment in Sc, Mn, Co, Sr and Te, suggesting a common enrichment process involving these elements. The REE pattern suggests a sedimentary origin for these schists, which were probably composed of clay mixed with components of volcanic origin.

In order to confirm the hydrothermal origin of the Praborna Mn ore deposit, we built up a database of more than 5000 data of modern hydrogenous and hydrothermal oceanic Mn deposits worldwide, adding data of oceanic Mn-rich sediments and of the Ligurian Mn ore deposits, which are thought to be the unmetamorphosed geological equivalent of Praborna. The classic ternary Mn–Fe–(Cu + Co + Ni) diagram, the agglomerative hierarchical clustering and the principal-component analysis, which takes into account a larger set of elements, strongly support the hypothesis of an oceanic hydrothermal origin for manganese in the Praborna and in the Ligurian ore deposits.

Key-words: manganese, trace elements, hydrothermalism, ocean floor, eclogite, blueschist, geochemistry, ore deposit.

1. Introduction

Fe- and Mn-rich shales and cherts have been known in ophiolite complexes for a long time. Well-known examples are those of Cyprus (*e.g.*, Constantinou & Govett, 1972) and eastern Liguria (Italy; Burckhardt & Falini, 1956; De Negri & Rivalenti, 1971; Cortesogno *et al.*, 1979; Marescotti & Cabella, 1996; Cabella *et al.*, 1998). After the rise of plate tectonics, they were soon recognised as equivalent to the Mn-rich deposits on the modern oceanic seafloors (*e.g.*, Bonatti *et al.*, 1976). However, a discussion arose on the origin and evolution of the few Mn ores associated with meta-ophiolites and strongly metamorphosed at high-pressure conditions, such as those of Praborna (Italy; this study) and Andros (Greece; *e.g.*, Reinecke, 1985). Their actual origin, hydrogenous (*i.e.*, sedimentary) or hydrothermal, is still debated, and the preservation of their chemistry during metamorphism is questioned.

Griffin & Mottana (1982) and Martin-Vernizzi (1982) suggested a hydrothermal origin for the Praborna proto-ore, on the basis of geochemical similarities with other Mn-rich deposits, especially the manganiferous cherts occurring in eastern Liguria to which Bonatti *et al.* (1976) had assigned a hydrothermal origin, later confirmed by Cabella *et al.* (1994), Marescotti & Cabella (1996) and Cabella *et al.* (1998). On this basis, Griffin & Mottana (1982) inferred that the Praborna ore body might have formed at an oceanic spreading centre, underlining the anomalies in Ba and Sr, the high Si/Al ratio of the Praborna rocks, and the abundance of sulphides in the underlying and nearby metabasites. To these arguments, Martin-Vernizzi (1982) added the structural position of the Praborna Mn-rich ore, which lies on hydrothermally

DOI: 10.1127/0935-1221/2010/0022-2035
0935-1221/10/0022-2035 $ 8.10

altered metabasites, and the proximity to the hydrothermal Fe–Cu deposit of Servette, hosted in meta-ophiolites (Martin *et al*., 2008).

Reinecke (1985) studied the Mn ore of Andros (Cyclades blueschist belt, Greece), an occurrence very similar to that of Praborna, but reached a different conclusion. Considering up to 9 elements (Mn, Fe, Co, Ni, Cu, Zn, As, Sr, Pb) in bulk-rock analyses, he compared the composition of the Andros Mn ore with those reported in the literature for present-day Mn nodules and their embedding sediments. He concluded that the Andros proto-ore should have consisted of hydrogenous Mn-nodule-, silica- and clay-rich oceanic sediments.

Thus, the precise source of the Mn deposits associated with meta-ophiolites is still debated, although their oceanic origin is generally accepted. However, the hydrothermal origin of the Praborna proto-ore should be reconsidered, as the enrichment in elements (Si, Mn, Ba, Sr) reported in the previous studies is insufficient to define its origin, these elements being sometimes even more concentrated in hydrogenous deposits (*e.g.*, Mn nodules) than in hydrothermal ores (Usui & Someya, 1997).

This article aims to provide a geochemical characterisation of the manganese deposit of Praborna. First, we give a presentation of the Praborna-ore occurrence and its geological setting. Then, we present major and trace analyses of 12 representative bulk rocks and selected minerals occurring at Praborna, including braunite and piemontite. In the discussion, we compare the data of the Praborna ore with those of modern geological environments, collected during recent seafloor-sampling projects, and with the analogous unmetamorphosed Ligurian Mn ores. This study is mainly based on trace-element analyses carried out with inductively-coupled-plasma mass spectrometry (ICP-MS). We report here also trace-element analyses carried out on selected minerals by means of secondary-ion mass spectrometry (SIMS). The large amount of analysed elements was treated by means of multivariate analysis (principal component analysis, PCA; agglomerative hierarchical clustering, AHC), together with more classical approaches such as normalisation spidergrams and ternary discriminating diagrams. In conclusion, we propose an updated hypothesis about the origin of the Praborna proto-ore and discuss the contribution of the rock-forming minerals to the geochemical characterisation of the deposit.

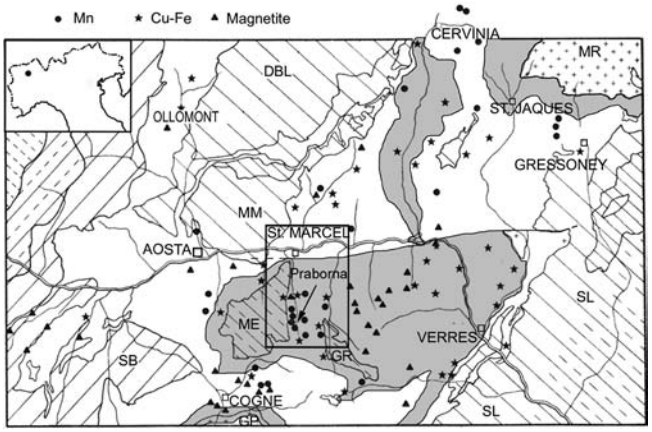

Fig. 1. Tectonic sketch map of the Aosta valley, showing Cu–Fe, Fe and Mn occurrences in the Piemonte Ophiolite Nappe (White unmarked: Combin unit. Grey unmarked: Zermatt-Saas unit). SB: Saint Bernard Nappe and Permo-Carboniferous Zone. GP and MR: Gran Paradiso and Monte Rosa Nappes. MM, DBL, ME and SL: Mount Mary, Dent Blanche, Mount Emilius and Sesia-Lanzo Austroalpine Nappes and Klippen.

2. Geological setting

2.1. The Piemonte meta-ophiolites

The Praborna Mn ore occurs within the meta-ophiolites of the Piemonte nappe, which extends along the entire arc of the Western Alps. Since the description of plate tectonics, these meta-ophiolites have been considered remnants of the oceanic lithosphere of the Ligure-Piemontese branch of the Tethys that opened in the Middle-Late Jurassic between the passive continental margins of Europe and Adria (Africa) (Dal Piaz, 1974; Compagnoni *et al.*, 1977; Dal Piaz *et al.*, 1979; see a historical review in Dal Piaz, 2001). This oceanic lithosphere was sliced and dismembered during the plate margin convergence that led to the subduction of the oceanic and continental slices under the Adriatic margin and to their partial exhumation. During the Alpine orogeny, the Piemonte ophiolite nappe was tectonically interposed between the underlying Pennine Monte Rosa – Gran Paradiso and the overlying Austro-alpine Sesia-Lanzo – Dent Blanche nappe systems (Fig. 1). On the basis of the metamorphic evolution of these meta-ophiolites, Dal Piaz (1965, 1974), Bearth (1967) and Kienast (1973) distinguished two main high-pressure units in the Piemonte nappe, the lower-grade Combin unit and the higher-grade Zermatt-Saas units (Fig. 1). The Praborna manganese ore, subject of this study, crops out in the Zermatt-Saas unit in the St. Marcel valley.

The rocks of the Zermatt-Saas unit are composed of serpentinite, ophicarbonate breccias, minor metagabbro with textural and/or mineralogical igneous relics, metabasalt with N-MORB affinity, and metasediments (*e.g.*, Martin *et al.*, 2004). The effect of oceanic hydrothermalism and alteration on the mafic rocks of the Zermatt-Saas unit is made evident by abnormal contents in various elements (Na, Mg, Ca) and H_2O (Beccaluva *et al.*, 1984; Barnicoat & Botwell, 1995; Martin & Cortiana, 2001), and the scattering of δO^{18} values (Cartwright & Barnicoat, 1999).

The formation of the Zermatt-Saas oceanic crust is attributed to the Jurassic (164–153 Ma; Rubatto *et al.*, 1998). Geochronology yielded a range of ages between 52 and 43 Ma (Eocene) for the subduction-related high-pressure metamorphism, depending on the technique used (Dal Piaz *et al.*, 2001, and references therein).

In this area, several Fe–Cu sulphide deposits occur in meta-ophiolites (*e.g.*, Dal Piaz & Omenetto, 1978). The most important Fe–Cu sulphide deposits occur in the Zermatt-Saas unit, within metabasalts (*i.e.*, garnet

glaucophanite, chlorite-schist, and talc-schist: see Martin *et al.*, 2008) that have undergone a strong oceanic alteration before high-pressure metamorphism.

Manganese deposits, occurring mainly as metamorphosed boudinaged quartzites and metacherts, have been described over the last century in the Alps (see extensive reviews in Dal Piaz *et al.*, 1979, and Mottana, 1986). These deposits have undergone a metamorphic overprint and structural reworking during the Alpine orogenesis, producing Mn-rich rocks composed of quartz, piemontite ($Ca_2Al_2Mn^{3+}Si_3O_{12}[OH]$), braunite ($Mn^{2+}Mn^{3+}SiO_{12}$) and spessartine garnet, often associated with Mn-bearing phengitic mica (''alurgite''), ± Mn-rich carbonates and other minor phases.

All manganese deposits show similar lithostratigraphic features. Rounded or flattened lenses of massive braunite represent the ore deposit in the manganiferous layers. These lenses are 1 cm to several m thick and appear black in colour. The gangue consists of single or repeated mm-to-m-thick, purple (piemontite-rich) or yellow (garnet-rich) layers containing variable amounts of quartz. The host quartz-rich metasediments are dominated by quartz + white mica ± garnet ± chlorite ± epidote ± albite ± carbonate.

The most important of many manganese deposits occurring in the Zermatt-Saas unit (Fig. 1) is that of Praborna.

2.2. The Praborna Mn ore

Praborna is located in the St. Marcel valley (Aosta valley, Italy; UTM coordinates: fuse 32, 3^{79} 50^{59}), where the well-known Cu–Fe mines of Servette and Chuc are enclosed within glaucophanite, chlorite- and talc-schists (Fig. 2 and 3; Martin *et al.*, 2008). In this area, also eclogite boudins were described by Martin & Tartarotti (1989).

Praborna is by far the most important and famous Mn occurrence of the Piemonte nappe. Known since 1415 (*e.g.*, Castello, 1982), described by de Saussure (1779–1796) and Bertrand de Lom (1844), it has been recently studied in detail by Martin-Vernizzi (1982), Martin & Kienast (1987), Mozgawa (1988) and Tumiati (2005). It is well known for very peculiar Mn-bearing assemblages (*e.g.*, Brown *et al.*, 1978; Mottana & Griffin, 1979, 1982; Griffin & Mottana, 1982; Martin-Vernizzi, 1982; Martin & Kienast, 1987; Mozgawa, 1988; Tumiati, 2005; Cenki-Tok & Chopin, 2006) and Sb-, As-, Ba-, Sr- and REE-rich minerals (*e.g.*, Perseil, 1988, 1998; Perseil & Smith, 1995; Smith & Perseil 1997; Perseil *et al.*, 2000; Tumiati, 2005; Cenki-Tok *et al.*, 2006). Praborna is the type locality for a score of mineral species, namely piemontite, braunite, romeite, manganiandrosite-(Ce) and strontiomelane (Ciriotti *et al.*, 2009).

The manganese deposit of Praborna is composed of a boudinaged quartz-rich layer, which extends over about 100 m and ranges from 0.4 to 8 m in thickness (4 m in Fig. 2). It is overlain by serpentinite, chlorite-schists and quartz-rich schists, contains a few intercalations of metapelites and metabasites, and lies on garnet + lawsonite glaucophanite (Fig. 2 and 3). The latter, locally retrogressed to greenschist-facies conditions (''prasinite''), contains abundant Cu–Fe sulphides, in a similar manner to the nearby Cu–Fe hydrothermal oceanic deposit of Servette–Chuc (*e.g.*, Martin *et al.*, 2008).

The metamorphic conditions of the manganese deposit are difficult to retrieve because conventional geothermobarometry and thermodynamic modelling cannot be straightforwardly applied to Mn-rich petrological systems (see Dasgupta, 1997). The presence at Praborna of glaucophanite with pseudomorphs after lawsonite indicates a *P–T* evolution across the lawsonite–blueschist subfacies during prograde metamorphism. The peak conditions of metamorphism in the St. Marcel valley have been estimated at Servette by Martin *et al.* (2008). The estimates of $P = 2.1 \pm 0.3$ GPa and $T = 550 \pm 60$°C would place the metamorphic peak into the amphibole-eclogite facies (following Liou *et al.*, 2004), transitional to the blueschist facies.

The Mn-rich layers are highly variable in terms of mineral assemblage, reflecting variations in bulk composition and oxidation state (Martin-Vernizzi, 1982; Mozgawa, 1988; Tumiati, 2005). They display numerous bands that alternate at different scales. Nevertheless, the layering is not laterally continuous (Fig. 3 and 4). At the mesoscale, the original layered structure appears deformed, resulting in isoclinal folds, boudinaged lenses and quartz-rich mylonite, transposed parallel to the foliation of the surrounding glaucophanite and serpentinite (Martin & Kienast, 1987). Despite the complex structure, a type sequence was recognised by Martin-Vernizzi (1982), Kienast & Martin (1983) and Martin & Kienast (1987). This sequence, slightly reorganised here (Fig. 2 and 3; Table 1), comprises, from bottom to top:

- Level 0: The footwall of the Mn-rich horizon is in contact with the underlying garnet-bearing glaucophanite, partially retrogressed to prasinite. Mica-schists and chlorite-schists also occur.
- Level 1: The basal Mn-rich level is a braunite- and clinopyroxene-rich layer. The pyroxene is a violet Mn-bearing omphacite–aegirine-augite solid solution (*i.e.*, the so-called ''violan'', Brown *et al.*, 1978). This level is highly fractured. Quartz, piemontite, clinopyroxene, Na–Ca amphibole and carbonate occur in minor amount. Along the fracture planes, Mn-rich phengite (''alurgite'', *cf.*, Brown *et al.*, 1978) occurs. Most of this level has now disappeared, as it was intensively mined for braunite.
- Level 2: this ore-body level is dominated by piemontite, braunite and quartz. Yellow layers of spessartine-rich garnet are common (Fig. 4a). In late fractures, albite, microcline, piemontite (II), Na–Ca amphibole and barite occur. As and Sb minerals, such as ardennite and romeite, can be found as accessory minerals.
- Level 3: this is an irregular emerald-green layer (10–20 cm), composed of quartz and Cr-bearing, aegirine-rich omphacite (Fig. 4b). This layer contains uncommon accessory phases, *e.g.*, native gold (Millosevich, 1906), Cr-rich epidote (with Cr near 1 atom per formula unit), Cr-rich muscovite (fuchsite), and very tiny (Ca, REE) vanadates, likely new

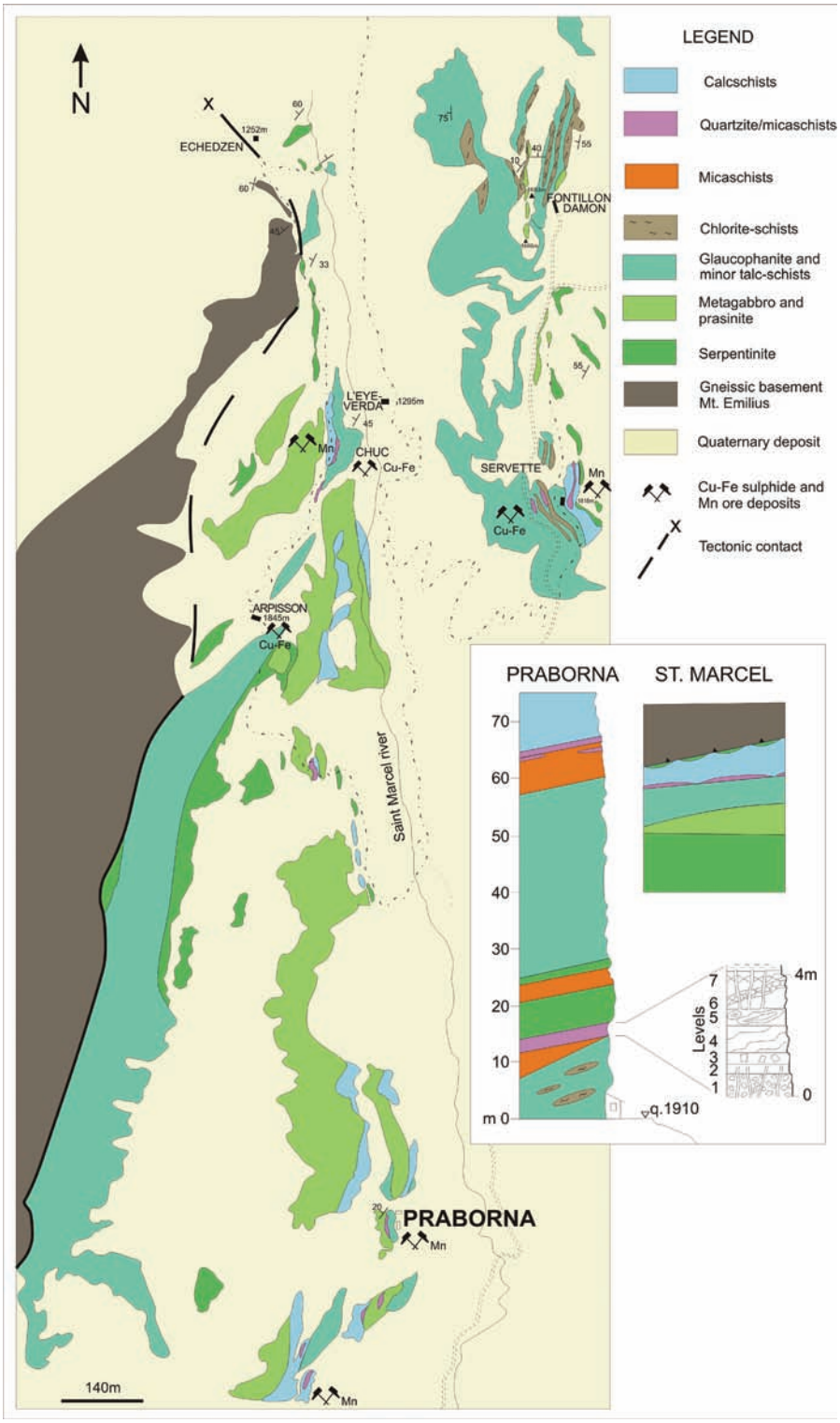

Fig. 2. Geological map of the St. Marcel valley. Cu–Fe and Mn mines are shown for reference. The schematic lithostratigraphy of the whole St. Marcel valley and the detailed sequence of Praborna are also reported. The numbering of the levels is consistent with Table 1 and Fig. 3.

mineral species with a (Ca + REE) *vs.* V ratio close to 1. The small dimension of these phases, which occur usually as <5 μm crystals intimately admixed with the matrix, prevented a more detailed characterisation. Further analyses are in progress.

- Levels 4, 5: these levels of Praborna contain calderite-rich garnet (Cenki-Tok & Chopin, 2006) and minor hematite in a quartz-rich matrix (level 4). In some cm-thick layers, garnet grows together with a

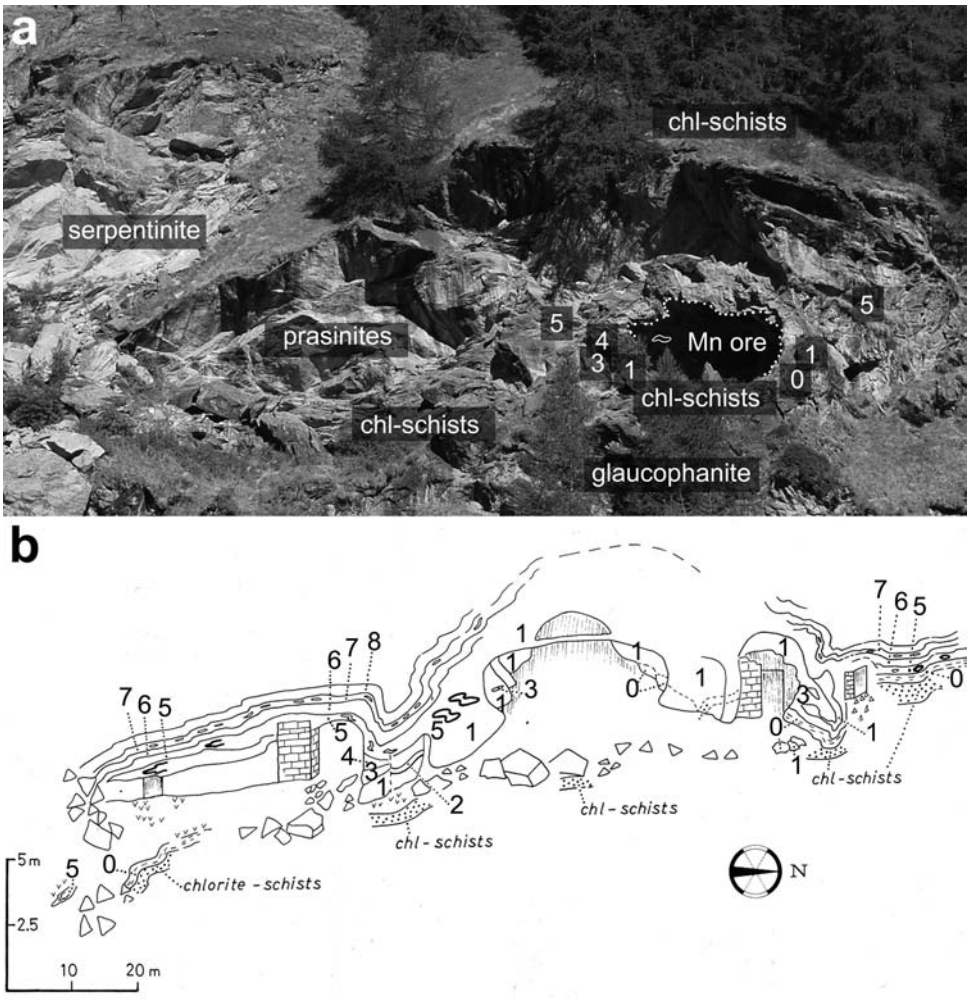

Fig. 3. Field view (a) and interpreted geological sketch (b), modified after Martin & Kienast, 1987 of the Praborna mine. Sequence numbering is consistent with Table 1 and Fig. 2.

brownish aegirine-rich clinopyroxene (level 5) and dark-green Na–Ca amphibole.

- Level 6: this outer level (Fig. 4c) is composed of cm-thick pinkish–orange boudins of quartz, pyroxmangite, strongly zoned garnet, and dark-coloured manganocummingtonite. Manganocummingtonite often shows weathering coatings of cryptomelane. Manganiandrosite-(Ce) and hematite occur as accessory minerals. Sb-rich pyrophanite developed after hematite.
- Level 7: the hanging wall of the ore, in contact with the country-rock, is composed of quartz, spessartine-rich garnet and Mn–Ca carbonates (rhodochrosite, kutnahorite). Some Na–Ca amphibole also occurs. Secondary Mn oxides and chlorite are also present.
- Level 8: the contact country-rock is a blueschist-facies quartz-rich schist (quartz + epidote + Na-amphibole + carbonate + phlogopite + garnet + hematite ± phengite; in the veins, albite + carbonate ± chlorite ± titanite).

The sequence seems to reflect a decrease in Mn oxidation state (*i.e.*, a decrease of the oxygen chemical potential) from the braunite–piemontite-rich footwall, where Mn^{3+} prevails, towards the spessartine- and carbonate-rich, Mn^{2+}-bearing layers of the hanging wall. Petrologically, we can distinguish four principal equilibrium assemblages:

- a primary, higher-*P* peak assemblage;
- an intermediate blueschist-facies retrograde assemblage;
- a late low-*P* greenschist-facies assemblage;
- weathering products.

The high-*P* peak assemblage is exceptionally well-preserved in the levels 1, 2 and 3 (the ''core'' of the mineralisation), with omphacite (''violan'' in level 1; emerald-green omphacite in level 3: Fig. 4) up to $Jd_{0.49}$ and phengite up to Si = 3.64 atoms per formula unit. The occurrence of piemontite (±Sr rich) is mainly confined in these core levels. Other minerals stable in the high-*P* peak assemblage are

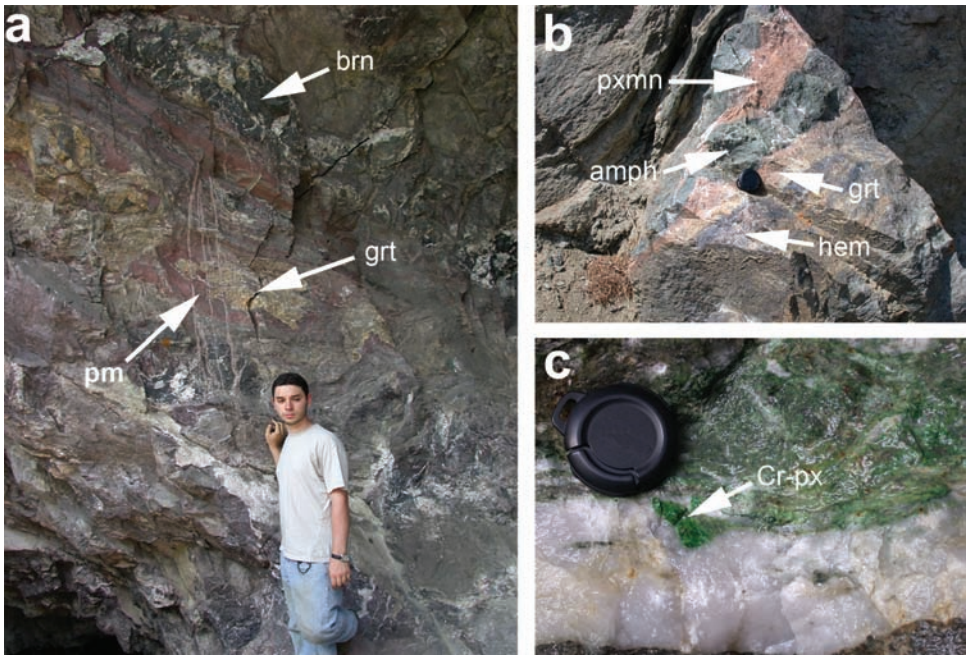

Fig. 4. Representative manganese-rich outcrops at Praborna; (a) preserved high-*P* assemblage (level 2): piemontite (pm) + garnet (grt) + braunite (brn); (b) retrogressed assemblage: pyroxmangite (pxmn) + manganocummingtonite (amph) + garnet (grt) + hematite (hem) (level 6); (c) Cr-rich level 3: Cr-rich clinopyroxene (Cr-px) in a quartz vein.

rutile (±Sb bearing), apatite (±As bearing), braunite, hollandite, hematite and ardennite.

Intermediate-*P* assemblages occur in the levels 1–3 mainly as symplectites after Jd-rich pyroxene (Jd-poor pyroxene + albite) and Si-rich phengite (Ba-rich K-feldspar + Mn-rich biotite), and as Na–Ca amphibole + albite associations. Piemontite also broke down into carbonate-bearing symplectites (Ba-rich K-feldspar + hollandite + calcite, minor witherite, strontianite and barite), probably linked to a late reaction with alkalis + CO_2-rich fluids (Tumiati, 2005). Intermediate-*P* conditions are displayed by the outer levels 4–8, characterised by the substantial absence of Jd-rich clinopyroxene and the abundance of calderite-rich garnet that becomes spessartine- and almandine-rich in proximity to the hanging-wall quartzite. Na–Ca amphibole (''crossite'', *i.e.*, winchite–riebeckite–barroisite–tremolite solid solutions) and/or aegirine/diopside-rich pyroxene can be present associated with garnet. Other phases are stable at these conditions: garnet, titanite (±Sb–As-rich), epidote (±REE–Cr–Sr-rich), (Ca, REE) vanadates, pyroxmangite, braunite, hematite, hollandite, pyrophanite (±Sb-rich), romeite, calcite (±Mn–Sr-rich), rhodochrosite and kutnahorite.

The low-*P* greenschist-facies assemblages, generally observed in late veins, are characterised by albite, quartz, K-feldspar, titanite, amphibole (tremolite), barite, rhodonite, calcite, strontianite, witherite and chlorite. Supergenic minerals are mainly restricted to weathering products and consist of Mn oxides and hydroxides such as manganite, birnessite and cryptomelane.

Some elements were remobilised within the deposit during its metamorphic evolution. Ba, for example, is found in minerals from the high-*P* peak (*e.g.*, hollandite, Ba-bearing piemontite), to the intermediate-*P* stage (*e.g.*, hyalophane after phengite) and the low-*P* greenschist facies (*e.g.*, barite in late albite-rich veins). We also observed a local remobilisation of As, Sb and REE, during a wide *P–T* range. These elements develop unusual minerals and mineral zonations from the peak metamorphism (*e.g.*, ardennite, Sb-rich rutile, As-rich apatite), to the intermediate-*P* step (*e.g.*, REE-zoned piemontite, romeite, Sb-rich titanite and pyrophanite, manganiandrosite-[Ce]), to the late greenschist facies (*e.g.*, As-rich manganite). Therefore, it can be assumed that the whole deposit behaved as an almost closed system during metamorphism.

3. Geochemical characterisation

3.1. Materials and methods

3.1.1. Bulk-rock chemistry

Previous data on the Praborna bulk-rock chemistry are very scarce. Only the unpublished work of Mozgawa (1988) reports a few analyses. In particular, the author analysed 6 samples of quartzite characterised by MnO ranging from 0.3 to 11.7 wt%. In addition to the major elements, he also analysed some trace elements by means of X-ray fluorescence, such as Cr, Ni, Cu, Rb, Sr, Zr and Ba. For just one sample, he reported also instrumental neutron-activation analyses of REE and other elements (Sc, Co, Ni, As, Sr, Sb, Ta, Hf, Th).

We selected 12 ore samples, whose mineralogy and petrology (Section 2.2) are described in Tables 1 and 2. Rocks 16/3, 17a, 3/03, 13/03, 14/03, 12/03 and 15/03 come from the preserved ''core'' of the mineralisation and display peak high-*P* mineral assemblages. Rocks 9/03, 1/03 and 5/03 display retrograde assemblages, mainly

Table 1. The type sequence of Praborna.

Levels	Lithology	Mineral assemblages	Mn oxidation state	Studied samples in this study	Comments	MK87 levels
8	Hanging-wall schists (Mn-poor)	Main assemblage: q + ep + Na-amph + carb + phl + grt + hem ± musc.Vein assemblage: ab + carb ± ti ± chl	−	4/03	Alm-rich garnet; amphibole is winchite-tremolite	h
7	Garnet + carbonate-quartzite	Main assemblage: q + grt + carb ± amph. Retrograde minerals: Mn-oxides, chl	2+	4/03	Spessartine-rich garnet; amphibole is winchite-tremolite	h–g
6	Pyroxmangite + garnet-quartzite	Main assemblage: q + pxmn + grt + amph; minor hem. Retrograde minerals: pyr (after hem), cry	2+	−	Sb-rich pyr; Manganiandrosite-(Ce); ambhibole is mangano-cummingtonite	g
5	Garnet-pyroxenite	Main assemblage: q + grt + Na-amph + cpx + rt ± brn. Retrograde minerals: ti, ilm, ab, Mn-oxides	2+	1/03; 5/03	Aeg-rich pyroxene; riebeckitic amphibole	f
4	Garnet-quartzite	Main assemblage: q + grt + carb + pyr ± pm. Retrograde minerals: Mn-oxides, chl (after grt)	2+, minor 3+	9/03	Calderite-rich garnet	e
3	Cr-rich quartzite (Mn-poor)	Main assemblage: q + cpx + phen+ rt ± pm. Retrograde minerals: amph, fuchsite (rims around phen), ep, ti (after rt), cc	3+	18/03	Gold; Ca vanadates; amphibole is winchite-tremolite	c
2	Ore-body quartzite	Main assemblage: pm + brn + q + hem + al ± grt ± rt. Retrograde minerals: ti (after rt), amph, kfs + phl (after al)	3+, minor 2+	3/03; 13/03; 14/03; 12/03; 15/03	Ardennite, romeite as occasional rock-forming minerals; amphibole is winchite-tremolite	b’
1	Ore-body basal pyroxenite	Main assemblage: cpx + brn + al + q + pm ± rt. Retrograde minerals: ab + cpx (II) (after cpx (I), ti (after rt), amph, kfs + phl (after al)	3+	16/03; 17a	Jd-rich pyroxene (cpx (I)); amphibole is winchite-tremolite; K-feldspar is Ba-rich (hyalophane)	b
0	Footwall glaucophanite (Mn-poor)	Main assemblage: amph + grt + rt + mt. Retrograde minerals: ep + musc (after lawsonite), ab, Ca-amph	−	−	Amphibole is glaucophane	a

Manganiferous layers are numbered 1 to 7. They lie on glaucophanite (level 0) and are overlain by quartz-rich schists (level 8). In the last column, we propose a comparison with the sequence of Martin & Kienast (1987) (MK87). Mineral abbreviations: q – quartz, ep – epidote, amph –amphibole, carb – carbonates, phl – phlogopite, grt – garnet, hem – hematite, musc – muscovite, ab – albite, ti – titanite, chl – chlorite, pxmn – pyroxmangite, pyr – pyrophanite, cry – cryptomelane, brn – braunite, rt – rutile, cpx – clinopyroxene, ilm – ilmenite, phen – phengite, pm – piemontite, al –‘‘alurgite’’ (*i.e.*, Mn-bearing phengite), kfs – K-feldspar, Jd – jadeite.

equilibrated under blueschist-facies conditions. Rock 18/03 represents the Cr-rich level 3, very poor in manganese. The Mn-poor quartz-rich schists at the hanging wall are represented by sample 4/03.

The chemical analyses (Table 3) were conducted by the *Service d’Analyse des Roches et des Minéraux* (SARM) of the CNRS (Nancy, France). Some additional ICP-MS analyses were performed on the same samples in the *Laboratorio di Chimica Analitica* (LCA) of the University of Insubria (Como, Italy) using the same analytical procedure. The details about the analytical methods and the declared analytical uncertainty and limit of detection for each element can be found *in* Carignan *et al.* (2001).

3.1.2. Mineral chemistry

Despite the abundance of published chemical analyses of minerals occurring at Praborna (see Section 2.2), only a few deal with trace and ultra-trace elements.

Although it is beyond the goal of this paper to describe in detail the crystal-chemistry of the mineral assemblages of Praborna, we provide representative analyses of selected minerals occurring in the ore as a reference for the discussion of bulk-rock analyses. We focused on manganese minerals from the high-*P* peak assemblage (levels 1 and 2; *cf.*, Section 2.2) because retrograde metasomatism should be minimal in this part of the ore. These minerals are piemontite, braunite, garnet, clinopyroxene and white mica (Table 4). Chemical analysis was performed using the Cameca SX100 wavelength-dispersive electron microprobe (EMP) of the University of Paris, with 15-kV accelerating potential, 15-nA sample current and 1-μm beam diameter. Standards used were albite (Na), diopside (Ca, Mg and Si), Fe_2O_3 (Fe), orthoclase (Al and K), $MnTiO_3$ (Mn and Ti), Cr_2O_3 (Cr) and barite (Ba). A counting time of 30 s was applied for all elements.

In Table 4, we neglect a series of accessory minerals (*cf.*, Section 2.2) because they are, in most cases, of minor

Table 2. Description of the samples selected for the bulk-rock analyses.

Sample	Lithology	Mineral assemblage	Metamorphic facies
16/03	Clinopyroxenite	Jadeitic clinopyroxene, quartz, braunite, phengitic mica	High-*P* peak
17a	Clinopyroxenite	Jadeitic clinopyroxene, piemontite, titanite	High-*P* peak
3/03	Mn-quartzite	Quartz, braunite, piemontite, minor garnet and phengitic mica	High-*P* peak
13/03	Mn-quartzite	Quartz, piemontite, braunite, minor garnet and phengitic mica	High-*P* peak
14/03	Mn-quartzite	Quartz, braunite, piemontite	High-*P* peak
39053	Mn-quartzite	Quartz, braunite, piemontite, minor garnet	High-*P* peak
15/03	''Piemontitite''	Piemontite; minor Na–Ca amphibole	High-*P* peak
18/03	Cr-bearing quartzite	Quartz, jadeitic clinopyroxene, minor phengitic mica and piemontite	High-*P* peak (Mn-poor)
9/03	Garnet-quartzite	Garnet, quartz, minor carbonates and secondary Mn-oxides	Retrogressed
1/03	Garnet-clinopyroxenite	Garnet, aegirine clinopyroxene, quartz, minor secondary Mn-oxides.	Retrogressed
5/03	Amphibole-garnetite	Garnet, Na–Ca amphibole, quartz;	Retrogressed
4/03	Quartzitic schist	Quartz, muscovite, garnet, Na–Ca amphibole, epidote, actinolite;	Retrogressed (Mn-poor)

Table 3. Bulk-rock analyses of selected samples from Praborna (see Tables 1 and 2).

	High-*P* rocks								Retrogressed rocks			Host schist
Element	16\03	17a	3\03	13\03	14\03	12\03	15\03	18\03	9\03	1\03	5\03	4\03
wt%												
SiO_2	54.61	54.56	54.1	87.69	65.28	45.65	43.29	72.48	63.23	61.61	52.65	75.05
Al_2O_3	15.89	9.86	3.52	0.68	3.63	7.17	10.63	6.04	9.86	7.54	12.26	7.87
Fe_2O_3	7.77	5.11	1.48	0.31	1.58	2.38	3.29	8.79	2.67	5.22	3.06	4.86
Mn_2O_3	2.7	3.42	30.49	9.44	19.7	38.74	13.59	0.18	19.08	14.62	20.21	0.61
MgO	2.38	5.99	0.82	0.26	0.84	0.58	3.98	1.62	0.64	1.99	1.88	1.79
CaO	1.28	10.5	4.7	0.5	4.45	3.11	15.45	2.85	4.1	4.94	5.15	3.99
BaO[a]	0.19	0.29	0.01	0.01	0.29	0.21	0.1	0.01	0	0	0.01	0.03
SrO[a]	0.04	0.37	0.2	0.01	0.88	0.04	1.82	0.01	0	0	0.01	0.04
Na_2O	6.86	6.42	0.33	<0.05	0.22	0.24	0.32	6.18	<0.05	2.24	2.24	1.3
K_2O	3.81	0.65	<0.05	0.23	0.38	<0.05	0.72	0.13	<0.05	<0.05	<0.05	1.44
TiO_2	0.6	0.48	0.17	<0.05	0.06	0.24	0.08	0.16	0.13	0.39	0.24	0.38
P_2O_5	0.08	0.04	0.06	0.04	0.04	0.08	0.27	0.25	0.05	0.06	0.13	0.16
L.O.I.	1.86	1.74	2.47	0.47	1.06	0.62	3.95	0.11	0.4	1.03	2.39	1.8
Total	98.07	99.42	98.34	99.64	98.49	99.12	97.49	98.8	100.16	99.64	100.23	99.32
CO_2	0.19	0.97	1.93	0.1	0.23	0.22	1.94	0.01	0.09	0.89	2.35	0.62
H_2O	1.42	0.47	0.43	0.23	0.42	0.19	1.5	0.18	0.21	0.27	0.37	1.11
F	0.08	0.01	0.01	<0.01	<0.01	0.01	0.053	0.02	0.01	<0.01	0.03	0.03
S	<0.01	<0.01	<0.01	<0.01	0.054	0.047	<0.01	<0.01	<0.01	<0.01	<0.01	<0.01
ppm												
Li	752	70	1	7	4	2	5	115	2	21	11	2
Be	1.9	2.1	<0.9	<0.9	<0.9	<0.9	0.7	1.6	<0.9	1.0	0.5	1.0
Cl	<20	32	<20	54	26	<20	21	<20	<20	<20	37	<20
Sc[b]	89	67	64	107	70	62	52	88	78	87	75	105
V	84	2.1	1.6	2.8	<1.5	4.0	8.2	62	14	49	120	134
Cr	25	15	12	15	12	26	67	468	13	42	35	76
Co	142	162	147	51	48	56	86	24	59	107	130	42
Ni	110	238	72	39	42	149	318	74	37	98	63	81
Cu	9	3	125	42	35	137	77	7	<5	<5	<5	<5
Zn	43	34	46	17	32	62	77	58	14	53	45	56
Ga	17.5	10.6	9.61	4.02	7.78	14.0	17.0	9.06	11.0	10.7	14.7	12.3
Ge	6.37	22.5	2.56	1.00	3.81	6.11	11.3	3.19	6.49	4.58	4.80	1.18
As	25	19	27	14	56	54	602	33	34	6.8	18	1.5
Rb	115	12	1	4	5	<1	11	24	<1	<1	<1	44
Sr	312	3147	1649	72	7467	301	15410	64	8	21	107	356
Y	3.99	3.87	11.0	1.60	4.64	15.5	10.2	1.98	20.7	8.49	20.5	23.7
Zr	124	66	27	6.3	17	40	16	48	37	33	52	78
Nb	13	17	0.7	0.2	0.2	3.2	0.6	3.3	0.3	2.6	1.1	5.8
Mo	1.01	<0.15	<0.15	<0.15	<0.15	0.84	<0.15	<0.15	0.96	<0.15	<0.15	<0.15

Table 3. Continued

	High-*P* rocks								Retrogressed rocks			Host schist
Element	16\03	17a	3\03	13\03	14\03	12\03	15\03	18\03	9\03	1\03	5\03	4\03
Ag[b]	0.060	0.190	0.170	0.020	0.390	0.050	0.960	0.060	<0.007	0.060	0.070	0.070
Cd[b]	<0.003	<0.003	0.080	<0.003	0.010	<0.003	0.110	<0.003	0.020	0.030	0.010	<0.003
In	<0.1	<0.1	<0.1	<0.1	<0.1	<0.1	<0.1	<0.1	<0.1	<0.1	<0.1	<0.1
Sn	2.7	1.4	0.6	<0.5	0.5	0.9	1.9	0.9	0.7	1.5	0.7	1.9
Sb	4.8	19	1.6	0.7	47	1.2	21	2.5	0.4	1.9	0.1	0.3
Te[b]	0.210	0.300	0.200	0.170	0.290	0.160	0.690	0.070	0.110	0.200	0.210	0.210
Cs	3.4	0.2	<0.2	<0.2	<0.2	<0.2	<0.2	<0.2	<0.2	<0.2	<0.2	1.1
Ba	1659	2564	76	104	2607	1863	890	47	42	6	66	235
La	7.5	6.00	15	0.66	6.8	11	40	0.73	1.4	0.89	0.73	28
Ce	49	31	27	5.4	11	38	46	2.1	3.7	3.2	2.3	63
Pr	2.1	1.9	3.1	0.18	1.8	2.7	8.9	0.23	0.40	0.49	0.27	6.9
Nd	8.0	8.0	12	0.76	6.9	9.7	36	1.0	1.7	2.5	1.5	27
Sm	1.2	1.8	2.4	0.28	1.3	2.1	7.0	0.28	0.97	1.1	1.3	5.7
Eu	0.23	0.35	0.52	0.07	0.29	0.54	1.5	0.07	0.54	0.47	0.66	1.3
Gd	0.88	1.2	2.2	0.31	1.0	2.3	5.4	0.28	3.0	2.3	3.1	5.0
Tb	0.13	0.15	0.33	0.04	0.15	0.42	0.56	0.05	0.56	0.33	0.56	0.75
Dy	0.74	0.80	2.0	0.24	0.85	2.6	2.1	0.32	3.4	1.6	3.5	4.3
Ho	0.16	0.14	0.43	0.05	0.17	0.51	0.27	0.07	0.65	0.28	0.73	0.80
Er	0.50	0.36	1.4	0.15	0.48	1.4	0.59	0.22	1.6	0.74	2.1	2.1
Tm	0.09	0.05	0.24	0.02	0.07	0.21	0.07	0.04	0.23	0.10	0.30	0.29
Yb	0.62	0.37	1.74	0.13	0.51	1.4	0.39	0.28	1.4	0.68	2.0	1.8
Lu	0.11	0.06	0.29	0.02	0.08	0.22	0.06	0.05	0.19	0.11	0.32	0.27
Hf	3.4	2.1	0.62	0.15	0.46	0.97	0.50	1.3	0.91	0.85	1.3	2.1
Ta	1.1	2.1	0.06	0.02	0.02	0.33	0.06	0.24	0.02	0.25	0.14	0.50
W	<0.1	<0.1	0.2	<0.1	<0.1	0.5	<0.1	0.3	0.3	1	0.6	0.4
Tl[b]	4.50	2.03	1.12	0.180	2.16	0.140	1.21	0.080	<0.004	0.030	0.010	0.640
Pb	11	17	20	<0.6	27	4.1	89	1.8	<0.6	<0.6	<0.6	21
Bi	<0.05	0.21	0.32	<0.05	<0.05	<0.05	1.0	<0.05	<0.05	<0.05	<0.05	0.37
Th	5.6	6.2	3.9	0.35	2.0	3.2	7.1	0.32	2.0	0.47	0.41	6.9
U	0.6	2	0.2	0.2	0.3	0.3	0.2	0.1	<0.1	<0.1	0.2	2

[a]recalculated oxides from trace-element analysis >1000 ppm.
[b]analysed by ICP-MS at University of Insubria (LCA).

interest concerning the major-element geochemistry of the ore. However, accessory minerals can be a sink of trace elements. A list of minerals that have been reported at Praborna rich in selected traces is shown in Table 5. In addition, we report for reference in Table 6 the composition of one of the most trace-enriched mineral, manganiandrosite, together with that of piemontite and braunite, the most abundant Mn-bearing phases occurring at Praborna. Trace analysis of minerals (Table 6) was performed by SIMS microanalysis in the University of Montpellier. The O^- primary beam (15 kV; 20 nA) was focused to sputter a flat-bottomed crater (25 μm diameter) on the sample. Before collecting secondary ions, the surface was sputtered for five minutes to remove the carbon coating. The surrounding carbon coat was sufficient to keep the surface from charging. Positive secondary ions for mass analysis were extracted with a 4.5-kV accelerating voltage. Secondary ions were detected by means of an electron multiplier operating in the ion counting mode. For the quantitative measurements of REE, the energy filtering technique was adopted using a 30-eV energy window, a high-energy offset of 80 eV, and fully open entrance and exit slits.

3.2. Results

Compared to the host rock, the manganiferous rocks cropping out at Praborna contain variable amounts of Mn, ranging from 2.7 to 38.74 wt% Mn_2O_3. The emerald-green level 3 (sample 18/03), although embedded in Mn-rich levels, is very poor in Mn, containing even less manganese than the Mn-poor quartz-rich schist occurring as the hanging wall of the manganiferous layers (sample 4/03) (0.18 wt% Mn_2O_3 *vs.* 0.61 wt% Mn_2O_3, respectively). According to Tables 1, 2 and 4, the major sink of manganese at Praborna are represented by braunite and piemontite in the preserved basal levels, and garnet in the retrogressed upper levels of the deposit.

In order to find geochemical anomalies, the bulk-rock analyses were normalised to the average shale composition (after Li & Schoonmaker, 2003) and compared with the

Table 4. Electron-microprobe analyses of major rock-forming minerals (sample 13/03, excepted for clinopyroxene, sample 17a), representative of the high-*P* assemblage of Praborna (see Table 1).

Oxides wt%	Braunite	Piemontite	Clinopyroxene	White mica	Garnet
SiO_2	9.87	36.84	55.60	50.33	36.99
TiO_2	0.05	0.03	0.06	0.16	0.24
Al_2O_3	0.08	19.97	7.35	26.27	19.57
Cr_2O_3	<L.D.	<L.D.	<L.D.	<L.D.	<L.D.
FeO	<L.D.	<L.D.	1.55	0.68	<L.D.
Fe_2O_3	1.76	3.11	6.32	<L.D.	1.09
MnO	11.40	3.63	0.78	0.66	34.37
Mn_2O_3	76.86	12.81	<L.D.	<L.D.	0.59
CaO	0.05	20.18	11.80	0.01	6.81
MgO	0.08	<L.D.	8.42	4.14	0.46
BaO	<L.D.	<L.D.	<L.D.	0.84	0.00
Na_2O	<L.D.	<L.D.	7.07	0.29	0.02
K_2O	<L.D.	<L.D.	0.14	10.42	0.00
Total	100.18	96.59	99.12	93.82	100.14
Elements (apfu)					
Si	0.991	3.032	2.015	3.419	3.000
Ti	0.004	0.002	0.002	0.008	0.015
Al	0.009	1.937	0.312	2.103	1.871
Cr	0.001	0.001	0.000	0.002	0.000
Fe^{2+}	0.000	0.000	0.047	0.039	0.000
Fe^{3+}	0.133	0.193	0.173	0.000	0.067
Mn^{2+}	0.969	0.253	0.024	0.038	2.361
Mn^{3+}	5.872	0.803	0.000	0.000	0.037
Ca	0.005	1.779	0.459	0.001	0.592
Mg	0.012	0.000	0.456	0.419	0.055
Ba	0.000	0.000	0.000	0.022	0.000
Na	0.004	0.001	0.496	0.038	0.003
K	0.000	0.000	0.006	0.903	0.000
Total cations	8.000	8.000	3.991	6.991	8.000
Anions	12.000	12.500	6.000	11.000	12.000
Fe^{2+}/Fe tot	0.00	0.00	0.24	1.00	0.00
Mn^{2+}/Mn tot	0.14	0.24	0.99	1	0.98

Formulae are calculated on the basis of anions. The Fe^{2+}/Fe^{3+} and Mn^{2+}/Mn^{3+} ratios were calculated iteratively by stoichiometry by fixing the number of cations. L.D. = limit of detection.

Table 5. Accessory minerals rich in selected trace elements described at Praborna.

Element	Accessory minerals
Ba	Hyalophane, hollandite, barite, witherite
As	Ardennite, titanite, apatite
Sr	Piemontite, strontiomelane, celestine, strontianite, calcite, manganiandrosite-(Ce)
Sb	Romeite, pyrophanite, rutile, titanite
REE	Piemontite, manganiandrosite-(Ce), (Ca, REE) vanadates
Cr	Clinopyroxene, muscovite, epidote
U, Th	zircon
V	(Ca, REE) vanadates
Cu, Zn, Co	Braunite, manganiandrosite-(Ce)
Ni	Piemontite, braunite, manganiandrosite-(Ce)

compositions of nodules (after Li & Schoonmaker, 2003), hydrogenous crusts and hydrothermal crusts (after Usui & Someya, 1997) (Fig. 5). The normalised data of the Mn-rich rocks were also compared with the hanging-wall schist (sample 4/03; Fig. 5).

The rocks of Praborna belong to layers displaying a range of compositions, resulting in the different mineral assemblages we described in Section 2.2. It is not clear whether this compositional banding is linked to a compositional primary character of the sedimentary protolith or it should be instead considered the expression of a complex metamorphic reaction front developed due to a geochemical gradient among the Mn deposit and the host rocks. Hereafter, we will refer to the average composition of the Praborna Mn-rich rocks, as this should correspond to the composition of the bulk deposit (red line in Fig. 5).

Compared to the reference shale, the Mn-poor quartz-rich schists of Praborna (represented by sample 4/03) are slightly richer in Na, Ca, Co, Sr and Te, and significantly so in Sc and Mn. They are poorer in Li, C, As, Sb, Cd and W.

The average composition of Praborna Mn-rich rocks is not significantly different from the Mn-poor schist for a series of elements: Be, C, F, Na, Ca, Mg, Al, Si, K, Sc, Ti, Fe, Ni, Zn, Sn, Te and W. For other elements, there is a

Table 6. Trace-element analyses of braunite, piemontite and manganiandrosite collected by secondary-ion mass spectrometry (SIMS). Piemontite and braunite come from the high-*P* part of the ore, while manganiandrosite is a retrograde mineral.

Element	Mean value (ppm)	±2σ	Detection limit (ppm)	Mean value (ppm)	±2σ	Detection limit (ppm)	Mean value (ppm)	±2σ	Detection limit (ppm)	Mean value (ppm)	±2σ	Detection limit (ppm)
	Piemontite (spot 1)			Piemontite (spot 2)			Braunite			Manganiandrosite		
P	937	142	50	104	17	16	51	60	10	201	32	23
Sc	11.5	0.5	1.1	9.2	0.8	0.9	5.1	0.2	0.6	13.6	0.6	1.1
V	1.1	0.2	0.6	1.2	0.2	0.6	1.4	0.5	0.6	46	1	4
Cu	84	13	17	16	3	7	2015	306	74	1393	210	69
Zn	361	56	72	211	46	54	1101	236	111	1676	257	153
Ga	217	33	21	77	12	12	237	135	19	183	28	19
Ge	0.24	0.04	0.06	0.23	0.04	0.06	0.10	0.02	0.04	9.4	1.5	0.9
As	459	75	101	238	39	71	76	16	36	n.a.	–	–
Rb	4.4	0.7	0.7	3.3	0.6	0.5	19	3	1	12	2	3
Sr	22,048	828	80	20,274	1,100	74	272	172	8	4998	188	37
Y	7.2	0.3	1.3	13.1	0.6	1.7	2.0	0.2	0.6	13.2	0.7	1.8
Nb	<L.D.	–	0.03	<L.D.	–	0.01	0.4	0.1	0.1	0.20	0.04	0.10
Sn	7.9	1.5	2.8	6.3	1.1	2.4	23	4	4	n.a.	–	–
Sb	<L.D.	–	1.5	n.a.	–	–	13	4	6	n.a.	–	–
Cs	<L.D.	–	0.04	<L.D.	–	0.02	<L.D.	–	0.05	<L.D.	–	0.03
Th	0.35	0.07	0.18	0.23	0.08	0.14	<L.D.	–	0.05	n.a.	–	–
Co	45	9	7	32	5	5	2543	390	41	1400	211	17
Ni	454	77	40	508	78	40	404	62	31	1801	271	36
Ba	767	63	56	27	3	10	194	167	23	22	2	6
U	n.a.	–	–	<L.D.	–	0.02	0.12	0.05	0.09	<L.D.	–	0.03
La	6.7	0.5	1.0	1.2	0.1	0.4	0.38	0.09	0.20	49748	2563	143
Ce	3.4	0.4	0.8	3.1	0.3	0.7	0.99	0.11	0.35	19754	21863	138
Pr	0.12	0.01	0.06	0.25	0.03	0.08	<L.D.	–	0.01	10873	352	66
Nd	4.2	0.5	0.9	5.2	0.5	1.0	0.07	0.03	0.10	37417	1700	346
Sm	0.18	0.05	0.17	0.64	0.11	0.31	0.33	0.03	0.19	2955	178	86
Eu	n.a.	–	–	0.08	0.03	0.08	nd	–	–	226	17	13
Tb	<L.D.	–	0.01	0.21	0.02	0.07	<L.D.	–	0.007	360	31	13
Gd	n.a.	–	–	0.65	0.11	0.25	<L.D.	–	0.007	2340	236	67
Dy	0.22	0.08	0.16	1.3	0.2	0.4	<L.D.	–	0.07	121	11	15
Ho	0.16	0.03	0.07	0.22	0.03	0.08	0.056	0.009	0.033	26	1	2
Er	0.52	0.07	0.27	0.43	0.07	0.23	0.27	0.04	0.16	314	26	26
Tm	0.12	0.01	0.06	0.03	0.01	0.03	0.07	0.01	0.04	18.3	0.9	1.3
Yb	0.40	0.07	0.25	0.25	0.06	0.19	0.63	0.09	0.26	n.a.	–	–
Lu	0.10	0.02	0.06	0.04	0.02	0.04	0.12	0.02	0.06	n.a.	–	–

n.a. = not analysed; L.D. = limit of detection.

marked differentiation. Mn-rich rocks, in addition to Mn, are richer in Co, Ge, As, Sr, Ag, Sb, Ba and Tl compared to the hanging-wall schist. Piemontite and braunite, occurring as major components in the basal levels (Tables 1, 2), can incorporate high amounts of traces, such as Sr and REE (piemontite) and the transition elements Co, Ni, Cu and Zn (braunite) (Tables 5 and 6). In the upper levels, close to the hanging wall, these elements can be accommodated into manganiandrosite (Tables 1 and 6).

Compared to the reference shale, the Mn-rich rocks are enriched in Na, Ca, Sc, Mn, Co, Ni, Cu, Ge, As, Sr, Ag, Sb, Te, Ba, Tl, Pb and Bi. They are poorer in C, Mg, Al, S, Cl, Ti, K, Cr, Fe, Zn, Ga, Rb, Y, Zr, Nb, Mo, Cd, Sn, Cs, REE, Th and U. Therefore, the enrichment in Na, Ca, Sc, Mn, Co, Sr and Te compared to the reference shale is shared both by Mn-rich rocks and the hanging-wall schists, suggesting a common enrichment process involving these elements. On the other hand, other elements seem to be characteristic of the Mn ore only: Ni, Cu, Ge, As, Ag, Sb, Ba, Tl, Pb and Bi.

The Mn-rich rocks are close in composition to average hydrothermal crusts with respect to S, Ti, Fe, Co, Ni, Cu, As, Y, Zr, Ag, Sb, Ba, REE, Pb and Nb (Fig. 5). However, compared to this type of deposits, they are characteristically depleted in some elements such as Li, V, Ni, Cu, Zn, Mo, Cd, W and U. Some elements appear to be much enriched: Al, Sc, Zr and Th. In particular, the Th/U ratio ranges from 1.63 in sample 13/03 to 42.21 in sample 9/03. The average Th/U at Praborna is 6.12, slightly higher than the reference shale (4.44) and the Praborna Mn-poor host schist (3.48).

The REE trend of the average concentration of Praborna Mn-rich rocks normalised to shale is slightly flat, plotting below reference shale (Fig. 5). Relative to modern Mn oceanic deposits, it is 14 times less concentrated in REE, which can be attributed to a dilution effect due to REE-free minerals,

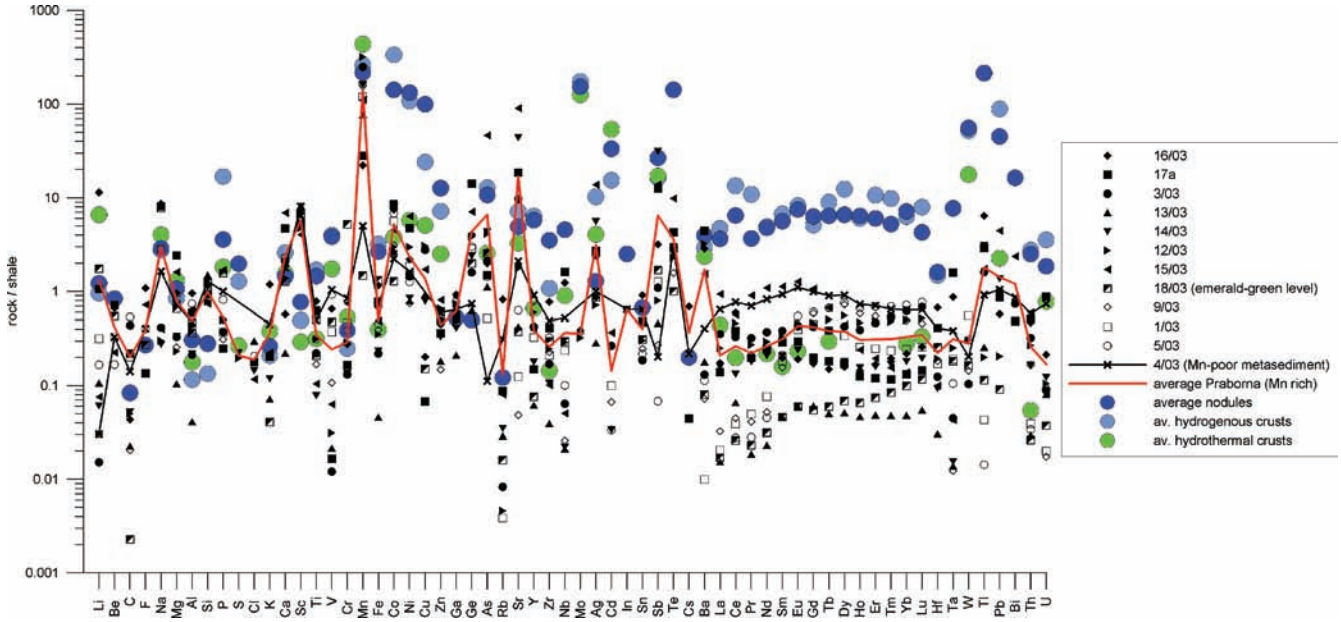

Fig. 5. Spidergram of the shale-normalised Praborna bulk-rock composition (*cf.* Table 3). The preserved high-*P* samples are represented with filled symbols, while the retrogressed samples are displayed with open symbols. The average composition of Praborna Mn-rich rocks is shown by a red line. The symbols of the Mn-poor hanging-wall schist 4/03 are connected with a black line. Normalization values and average data for shale and hydrogenous nodules (dark blue circles), shown for reference, are from Li & Schoonmaker (2003). Average data of Pacific hydrogenous crusts (light blue circles) and modern hydrothermal crusts (green line circles) are from Usui & Someya (1997).

such as quartz. The REE pattern multiplied by 14 (Fig. 6) is comparable to deposits characterised by 20 % hydrogenous and 80 % hydrothermal contributions, according to the model of Fleet (1983). The Mn-poor host schist of Praborna displays more or less the same REE pattern (Fig. 6), despite a higher REE content close to the reference shale. This suggests that the Mn-enrichment process did not modify the REE signature of the protolith. The flat REE pattern for both Mn-poor and Mn-rich rocks strongly suggests a sedimentary origin for Praborna rocks. The moderate middle-REE (MREE) enrichment, with a regular increase in REE from La to Eu, could be attributed to volcanic glass in the sediment (Frey *et al.*, 1974).

4. Discussion

The major- and trace-element data collected during this study allow a comparison between Praborna and modern oceanic Mn deposits in order to unravel the nature of the proto-ore. For this purpose, we adopted a multivariate statistical approach, principal component analysis (PCA) and agglomerative hierarchical clustering (AHC), to the bulk-rock data presented in Section 3.1.1.

4.1. Modern oceanic Mn deposits: an overview

Mn deposits, typically nodules or crusts, are nearly ubiquitous on the seafloor (Manheim, 1978; Roy, 1981; Hein *et al.*, 1987; Usui *et al.*, 1989), particularly on the topographic highs where the supply of terrigenous, volcanogenic and biogenic components is very low (Usui & Someya, 1997). Similar fossil Mn deposits have also been found, albeit much less common, within drill cores of the Deep Sea Drilling Project (DSDP)/Ocean Drilling Project (ODP), in sediments as old as the late Cretaceous (Glasby, 1978; Usui & Ito, 1994).

For many years, the origin of these Mn nodules and encrustations remained controversial, between submarine volcanism and continental runoff (Murray & Renard, 1891). More recently, the formation of these nodules was reinterpreted in the light of the plate-tectonic theory. Bonatti *et al.* (1972) attempted a qualitative classification of Fe–Mn oxide deposits on the basis of potential sources of elements: (i) hydrogenous, deriving from slow precipitation from normal seawater; (ii) hydrothermal, resulting from the hydrothermal activity in areas of high heat flow associated with volcanism; (iii) halmyrolitic, deriving, at least in part, from the submarine alteration of the basaltic seafloor and (iv) diagenetic, resulting from a post-depositional redistribution within the sediment column.

The mineralogy, crystallography and mineral chemistry of manganese deposits and mineral chemistry are still controversial, since Mn oxides are usually poorly crystalline or amorphous. Most deposits contain a mixture of amorphous iron oxyhydroxide, δ-MnO_2 (occasionally called ''vernadite''), other rarer MnO_2 minerals (pyrolusite, ramsdellite and nsutite), birnessite ($(Na,Ca)_{0.5}(Mn^{4+},Mn^{3+})O_2{:}1.5\ H_2O$), todorokite ($(Mn^{2+},Mg,Ca,Ba,K,Na)_2Mn^{4+}{}_3O_{12}{:}3H_2O$), occasional α-FeOOH (goethite) and γ-FeOOH (lepidocrocite) (Aplin, 2000). Birnessite and todorokite have a double layer structure consisting of

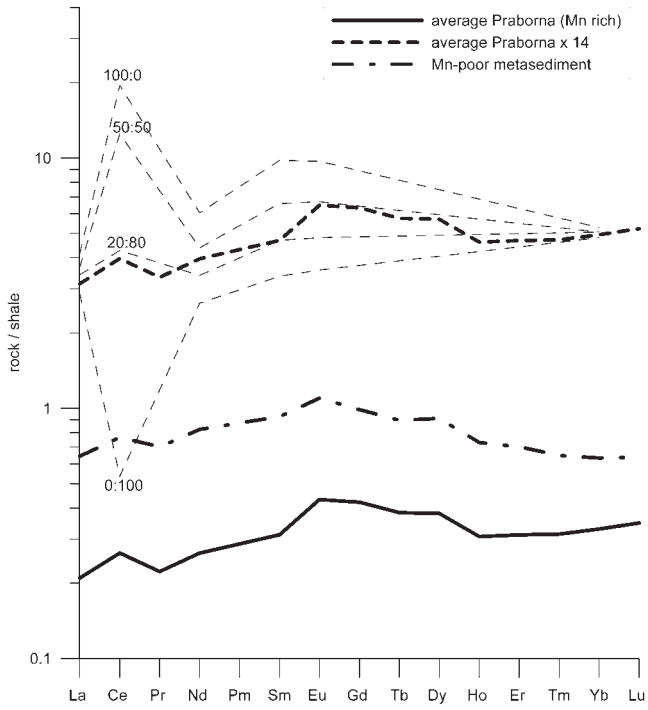

Fig. 6. Shale-normalised REE in the Praborna bulk rocks. Normalisation values were taken after Li & Schoonmaker (2003). REE concentration of the Mn-rich rocks multiplied by 14 is also shown (see text for details). The patterns are superposed on hypothetical mixtures of average hydrothermal material and average hydrogenous ferromanganese material proposed by Fleet (1983). The first and second values in ratios represent the percentages of hydrogenous and hydrothermal material respectively. According to this model, Praborna reflects about 80 % hydrothermal input.

ordered sheets of MnO_2 with disordered layers that can incorporate transition elements such as Mn^{2+}, Cu^{2+}, Ni^{2+} and Fe^{2+}, coordinated with O^{2-}, OH^- and H_2O. In these complex crystal structures, significant amounts of other elements such as Mg, K, Ba, Na and Ca can enter (Aplin, 2000).

Cronan (1980), Aplin & Cronan (1985) and Aplin (2000) proposed a new classification of the various oceanic Fe–Mn deposits according to their environment and composition:

(i) Hydrogenous Fe–Mn crusts: these crusts, which accrete directly from seawater and are not influenced by hydrothermal activity, contain mainly δ-MnO_2 and iron hydroxides. They have Mn/Fe ratios around 1 and are rich in Co compared to other trace metals such as Cu, Ni and Zn.

(ii) Hydrogenous Fe–Mn-nodules: their composition strongly depends on the extent to which metals are accreted either directly from the water column or from the sediment-pore water. Nodules form by precipitation of Mn^{2+} as β-MnO_2, in oxidising and neutral conditions (*i.e.*, Eh $\approx$ 0.5, pH = 7). They also become enriched in Cu, Ni and Zn as a result of their release from decaying organic matter. The Mn/Fe ratio of these nodules ranges from 2 to 7. These nodules contain todorokite, implying a degree of reductive remobilisation of primary Mn oxides and their subsequent re-precipitation within nodules.

(iii) Encrustations on rocks close to hydrothermal vents (sometimes referred to as ''hydrothermal crusts''): they are composed of oxides that usually show very high Mn/Fe ratios as a result of the preferred incorporation of Fe into sulphide or silicate minerals at the vents of the hydrothermal system. Compared with hydrogenous Fe–Mn deposits, which grow at around 1 mm/Ma, hydrothermal deposits accrete rapidly. Despite the fact that they contain abundant todorokite, which can readily incorporate transition metals, the rapid growth of ''hydrothermal crusts'' appears to prevent the uptake of significant amounts of trace metals. Compared with hydrogenous crusts, they are depleted of all trace metals.

4.2. The origin of manganese at Praborna

In order to analytically describe the similarities among the analysed rocks and hydrogenous nodules, hydrogenous crusts and hydrothermal crusts (Fig. 5), we applied agglomerative hierarchical clustering using the statistical software XLSTAT by Addinsoft (http://www.xlstat.com/). This iterative classification method is based on the calculation of the dissimilarities between objects (Everitt *et al*., 2001). The objects whose clustering together minimises the agglomeration criterion are then clustered together. These successive clustering operations produce a binary clustering tree (hierarchical clustering dendrogram; Fig. 7), whose root is the

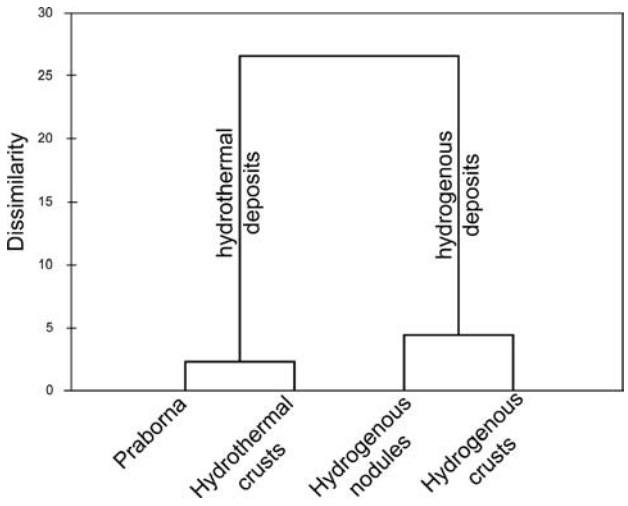

Fig. 7. Agglomerative hierarchical clustering of manganese deposits and Praborna Mn-rich rocks. The dendrogram was generated using the software XLSTAT. The considered dissimilarity coefficient is the Euclidean distance; the agglomeration method was that of Ward (Everitt *et al*., 2001).

class that contains all the observations. Following this method, the Mn-rich rocks of Praborna were grouped together with hydrothermal crusts, indicating that they share more geochemical characters with this type of deposits rather than with hydrogenous deposits.

As seen in Section 3, the REE pattern also suggests that the Praborna deposit is dominated by hydrothermal contributions. However, compared to the ''average'' composition of hydrothermal crusts, Praborna displays different content in some elements, such as W, Cd, Zn, V, Mo, Cu and Ni (Section 3.2; Fig. 5). This could reflect a primary character of the ore. Actually, the hydrothermal crusts display a wide range of compositions (Usui & Someya, 1997). Mo, for example, ranges from 27 to 1840 ppm. V varies from 93 to 1019 ppm. Also the Th/U at Praborna (6.12) differs from the average hydrothermal value of 0.31, calculated using the data of Usui & Someya (1997). This high ratio might have been inherited from the sedimentary part of the ore, since the host Mn-poor schist displays a high Th/U (3.48 in sample 4/03). Furthermore, even if Th/U in the Praborna Mn-rich rocks seems to be high, the low absolute contents of Th (0.35–7.09 ppm; average 2.60 ppm) and U (0.05–2.36 ppm; average 0.42 ppm) are still in the compositional range of hydrothermal crusts (Th = 0.03–6.63 ppm; U = 0.2–10.1 ppm; after Usui & Someya, 1997), whereas hydrogenous deposits are characterised by higher contents in Th and U.

The principal component analysis (PCA) was performed on a dataset built from the following sources:

(i) the excellent database of Usui & Someya (1997), with average analyses of major and trace elements for both hydrogenous and hydrothermal Mn deposits from the north-western Pacific;
(ii) the Central Data Repository of the International Seabed Authority (ISA), available on-line (http://www.isa.org.jm) and continuously in development, it comprises major- and trace-element compositions and depth of hydrogenous polymetallic nodules, unclassified Fe–Mn crusts, and hydrothermal deposits of various origins;
(iii) geochemical data on hydrothermal Mn crusts from the Indian Ocean (Nath *et al.*, 1997);
(iv) the core database of the Ocean Drilling Project (ODP; Legs 101–129), available on-line (http://www.ngdc.noaa.gov/mgg/geology/drill.html). It provides X-ray-fluorescence chemical analyses of oceanic sediments and basement rocks. We selected those sediment analyses with MnO > 1 wt%.

The resulting database was compared with the fossil oceanic deposits from (a) Praborna (Table 3 + bulk-rock analyses of Mozgawa, 1988), and (b) Ligurian Mn ores (Marescotti & Cabella, 1996; Marescotti, 1997), which are thought to be analogous to the Praborna proto-ore, lacking the Alpine metamorphic overprint.

Data of sulphide-rich, Mn-poor ores were filtered, only considering analyses with S < 2 wt% and MnO > 1 wt%. A total of 5360 data, including Praborna, build up the final database, freely available online as Supplementary material (Table S1) linked to this article on the GSW website of the journal: http://eurjmin.geoscienceworls.org/.

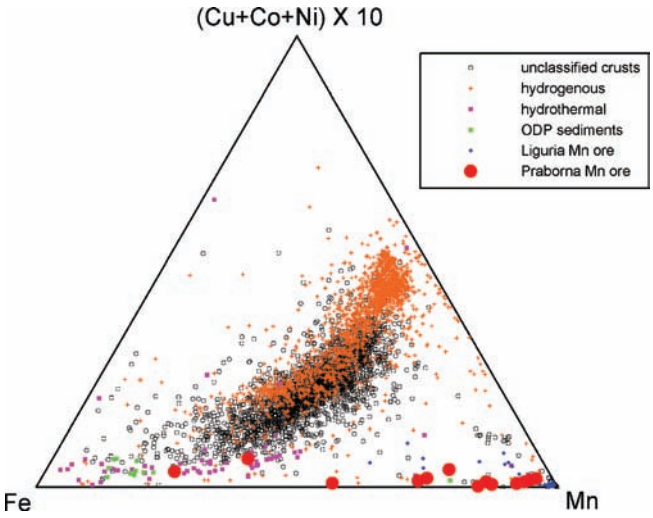

Fig. 8. Mn–Fe–(Co + Ni + Cu) × 10 ternary diagram of hydrogenous and hydrothermal Mn-rich deposits. Data of Praborna and Liguria ores and ODP sediments are also displayed. See text for further details.

Mn oceanic deposits are often characterised by the classical Mn–Fe–(Cu + Co + Ni) × 10 ternary diagram proposed by Bonatti *et al.* (1972). In this diagram, generated with the described dataset, the samples from Praborna lie in the (Co + Cu + Ni)-poor region, typical of hydrothermal deposits (Fig. 8). Analyses of the Ligurian ores, Indian Ocean crusts and ODP Mn-rich sediments also plot in this region.

In addition to this classical approach, we applied principal component analysis (PCA) to our database, taking Praborna, ODP sediments and Ligurian analyses as complementary data (*i.e.*, not considered while performing the PCA). The considered elements (Na, Mg, Al, Si, P, K, Ca, Ti, V, Cr, Mn and Fe as major elements; Co, Ni, Cu, Zn, As, Sr, Y, Zr, Mo, Ba, La, Ce and Pb as trace elements) were chosen for their completeness throughout the database (missing data <5000 over 5360). For the calculations, the remaining missing element data were estimated by the nearest-neighbour method using the software XLSTAT. To counteract artefacts introduced by this estimation, PCA observation weights were inversely proportional to the number of missing analyses raised to the power of two. The weights of the data from Usui & Someya (1997), being average data of a huge number of samples, were chosen equal to the declared number of averaged samples. The complete database used for the PCA is available online as Supplementary material (Table S1).

PCA transforms a number of correlated variables (Mn, . . . , Sr) into uncorrelated variables called principal components (F_1, . . ., F_{25}), the coordinates of which in the initial basis (Mn, . . ., Sr) are provided by the eigenvectors of the correlation matrix (Tables S2 and S3, respectively, in Supplementary material). The greatest variance comes to lie on the first principal component (F_1), the second

greatest variance on the second (F_2), and so on, the importance of these variances being given by the corresponding eigenvalue (Table S2 in Supplementary material). In order to reveal possible correlations, the data vectors (bulk-rock analyses) and the initial variables (Mn, . . ., Sr) are projected on binary diagrams F_n - F_m (biplots: Fig. 9). The coordinates of the initial variables in a biplot gives their contribution to the corresponding variances. Because the variable vectors (Mn, . . ., Sr) are normalized in the new basis (F_1, . . ., F_{25}), the apparent norm of these vectors in a biplot is limited (to 10 in Fig. 9).

The principal component F_1 (Fig. 9), which accounts for 57.29 % of the total eigenvalues, represents mainly an anti-correlation between Fe and Mn. Therefore, this axis roughly corresponds to the Fe–Mn side of Bonatti's triangle.

Component F_2 (Fig. 9; 15.70 % of the eigenvalues) represents the enrichment in Si + Al (+Na), most probably related to the occurrence of clay minerals and other silicates. Along this vector, the alumino-silicate (pelitic) fraction in the sediment increases. It is worth underlining here that the Si/Al ratio has been used to distinguish between hydrothermal Fe–Mn crusts, rich in Si and characterised by a Si/Al ratio > 5.1, and nodules, whose typical Si/Al ratio is 3, the same as marine sediments (Toth, 1980). Praborna displays a Si/Al average ratio of 16.35, thus being of hydrothermal origin according to this criterion.

Component F_3 (Table S2; 7.01 % of the eigenvalues) represents most probably the phosphate richness of the deposits. As reported by Baturin & Yushina (2007), the correlation between Ca and P in oceanic Mn deposits suggests that phosphorus occurs as apatite.

Component F_4 (Fig. 9; 5.43 % of the eigenvalues) represents a strong correlation among Cu, Ni, Zn and Co. This would correspond to the upper apex of Bonatti's triangle. The result of the PCA suggests that Co is not as effective as Cu + Ni + Zn in distinguishing among the different types of Mn deposits. A Co-free triangle (Fe–Mn–[Cu + Ni] × 10: *cf.*, Usui & Someya, 1997) or, better, a Zn-bearing triangle (*e.g.*, Fe–Mn–[Cu + Ni + Zn + Co] × 10) could be used instead. The Co/Zn ratio was used by Toth (1980) as an indicator of hydrothermal genesis. Hydrothermal deposits display a mean value of 0.15, whereas hydrogenous deposits show a mean value of 2.5. The Praborna mean Co/Zn ratio is 2.48. Therefore, considering this parameter alone would place Praborna in the hydrogenous field.

The 21 other principal components (F_5, . . ., F_{25}), which account for less than 16 % of the total eigenvalues, are considered negligible.

REE are positively correlated along F_1, together with Fe and the transition metals. They are anti-correlated with Mn (Table S3). REE have been classically used to classify Mn deposits. In particular, Toth (1980) reported a La/Ce ratio close to seawater (2.8) for hydrothermal deposits, while hydrogenous deposits show ratios as low as 0.25. Praborna displays a mean La/Ce of 0.38. Again, this simplicistic approach would place Praborna in the hydrogenous field. However, if we consider Co + Ni + Cu *vs.* $\sum$REE (Clauer *et al.*, 1984), Praborna plots in the hydrothermal field, characterised by relatively low contents of all these elements. The REE are also slightly anti-correlated with Si (Fig. 9), which can be attributed to the dilution effect of quartz (see also Fig. 6).

In conclusion, PCA can well distinguish pure ores from ores admixed with an alumino-silicic gangue (F_2). Both pure, massive hydrogenous and hydrothermal deposits are poor in elements such as Na, Si, Mg, K and Al (positive

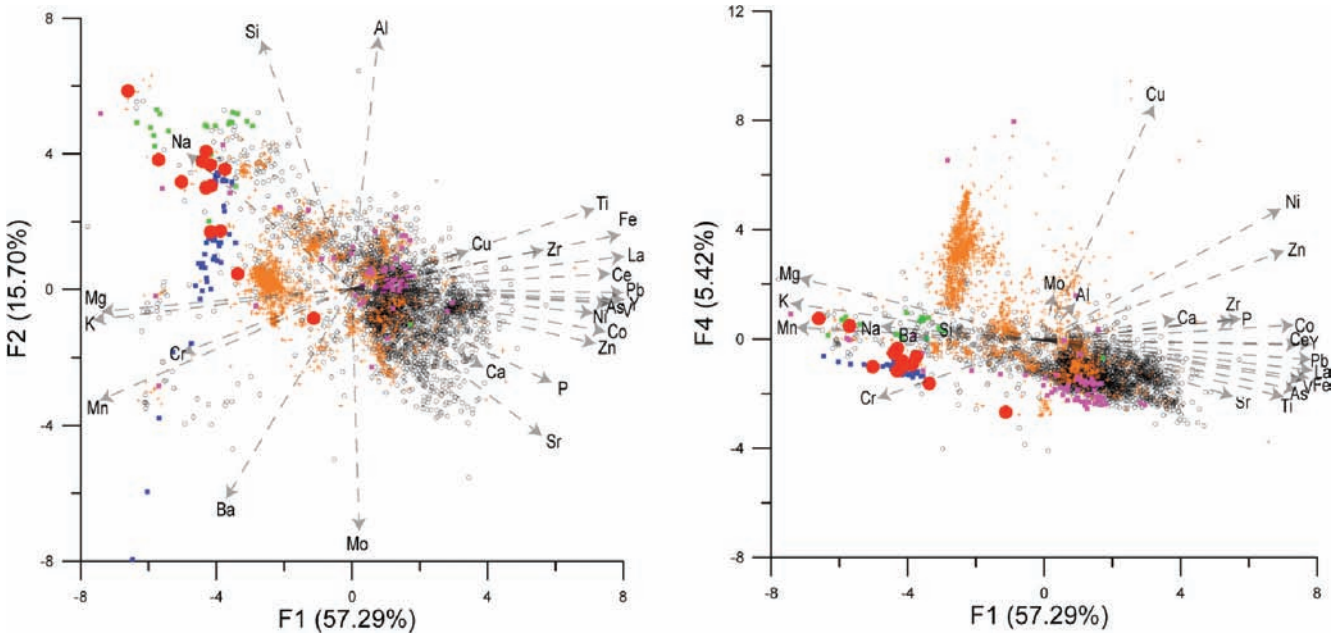

Fig. 9. Principal component analysis. Data and symbols are the same as in Fig. 8. The norm of the initial variable vectors (Mn, . . ., Sr) is multiplied by 10. See text for further details.

F_1). On the contrary, the ores from Praborna (red circles in Fig. 9) and Liguria (blue circles in Fig. 9) are rich in these elements, ascribable to minerals such as quartz, clays, micas and other silicates, which shift the bulk composition close to that of the ODP sediments (green circles in Fig. 9). Compared to hydrothermal deposits, hydrogenous ones are richer in Fe, transition metals and REE (higher values of F_1 and F_4). Praborna and Liguria are closely related to hydrothermal deposits, displaying even negative F_4 values. ODP sediments display relatively high F_4 values, suggesting a higher hydrogenous contribution (Mn-rich nodules?).

5. Conclusions

Comparing the Praborna rocks with modern oceanic Mn ore and sediments leads to the conclusion that Praborna is far removed in composition from hydrogenous crusts or nodules. On the contrary, it shows analogies to Mn–Fe-rich hydrothermal oceanic crusts. The low S-content in the Praborna ore deposit indicates that the latter formed at some distance from the hydrothermal source, where sulphides would form, as in the neighbouring Chuc-Servette deposit (Section 2).

Because of its thickness (up to 8 m), the Praborna occurrence could hardly derive from hydrogenous crusts or nodules, whose growth is generally very slow (around 1 mm/Ma: Aplin, 2000). This latter origin cannot be excluded for some cm-to-dm-thick Mn-rich outcrops that are common in metaophiolites (*e.g.*, on Andros).

The Praborna Mn-rich sequence is heterogeneous regarding chemistry and mineralogy. However, the composition of the various layers partly follows the trend observed in modern Fe–Mn deposits. We can conclude that the geochemical signature was preserved during the high-pressure metamorphism. On the other hand, the Praborna samples show that trace elements and REE are linked to the sample mineralogy to some extent. As the mineralogy is controlled by the major-element composition, these correlations likely indicate a partial redistribution of trace elements and REE at the sample (or outcrop) scale during metamorphism. The prevailing occurrence of Mn^{3+}-bearing phases (piemontite, braunite) in the high-*P* peak assemblage of the preserved ''core'' of the ore body indicates that the high oxygen chemical potential was at least partially conserved during the metamorphism of the Mn^{4+}-bearing phases typical of oceanic Mn deposits (birnessite, todorokite).

The Mn-rich ore body is hosted by schists derived from silica-rich claystones with some volcanogenic components. The basement was made of hydrothermally altered basalts (now glaucophanite) and serpentinite. This scenario indicates that the Mn deposit of Praborna could well be the high-*P* metamorphosed equivalent of the Jurassic Mn-rich cherts that crop out in the Northern Apennines. In both deposits, the ore mineral is now braunite. Both Praborna and the Liguria ore deposits show many geochemical similarities with modern hydrothermal Mn-rich crusts found on the present-day oceanic floor.

Acknowledgements: The authors are indebted to the reviewers Piergiorgio Rossetti and Giorgio Garuti, and the editors Carlos Ayora and Sandro Conticelli, whose suggestions significantly improved the manuscript. We also thank Pietro Marescotti and Roberto Cabella (University of Genova) who provided some unpublished data of the Ligurian ores. Bernard Boyer (University of Montpellier) provided assistance at SIMS and Michel Fialin (University of Paris) supported the work at EMP. We are grateful to Damiano Monticelli and Elena Ciceri (University of Insubria) for the ICP-MS analysis. Nicola Michelon is thanked for his help in drawing Fig. 2. We also thank Nancy Yenkins for the English corrections. The study was sponsored by the Saint-Marcel municipality within the project INTERREG IIIA 2000–2006 Italy–France (ALCOTRA) and partially funded by ERDF funds in the framework of the EU Community Initiative INTERREG III B Alpine Space Program–project IRON ROUTE. S.T. was supported by a fellowship given by the *Istituto della Montagna* (ex INRM, Rome, Italy).

References

Aplin, A. (2000): Mineralogy of modern marine sediments: a geochemical framework. *EMU Notes Mineral.*, **2**, 125–172.

Aplin, A. & Cronan, D.S. (1985): Ferromanganese deposits from the central Pacific Ocean: I. Encrustations from the Line Islands Archipelago. *Geochim. Cosmochim. Acta*, **40**, 427–436.

Barnicoat, A.C. & Botwell, S.A. (1995): Seafloor hydrothermal alteration in metabasites from high-pressure ophiolites of the Zermatt-Aosta area of the western Alps. *Boll. Mus. Sci. Nat. Torino*, **13** (Suppl.), 191–220.

Baturin, G.N. & Yushina, I.G. (2007): Rare earth elements in phosphate–ferromanganese crusts on Pacific seamounts. *Lithol. Min. Res.*, **42**, 101–117.

Bearth, P. (1967): Die Ophiolithe der Zone von Zermatt-Saas Fee. *Beitr. geol. Karte Schweiz*, **NF132**, 130 p.

Beccaluva, L., Dal Piaz, G.V., Macciotta, G. (1984): Transitional to normal MORB in ophiolitic metabasites from the Zermatt-Saas, Combin and Antrona units, western Alps: implications for the paleogeographic evolution of the western Tethyan basin. *Geol. Mijnbouw*, **63**, 165–177.

Bertrand de Lom, J.-P. (1844): Description minéralogique et géologique de la mine de manganèse de Saint-Marcel en Piémont, et de quelques faits du même genre de la vallée où gît cette mine. *Echo du Monde savant*, **11/21**, 487–495.

Bonatti, E., Kraemer, T., Rydell, H. (1972): Classification and genesis of submarine iron-manganese deposits. *in* ''Ferromanganese deposits of the ocean floor'', D.R. Horn, ed. National Science Foundation, Washington D.C., 149–165.

Bonatti, E., Zerbi, M., Kay, R., Rydell, H.S. (1976): Metalliferous deposits from the Apennine ophiolites: Mesozoic equivalent of modern deposits from oceanic spreading centre. *Geol. Soc. Am. Bull.*, **87**, 83–94.

Brown, P., Essene, E.J., Peacor, D.R. (1978): The mineralogy and petrology of manganese-rich rocks from St. Marcel, Piedmont, Italy. *Contrib. Mineral. Petrol.*, **67**, 227–232.

Burckhardt, C.E. & Falini, F. (1956): Memoria sui giacimenti italiani di manganese. *in* ''Symposium sobre yacimientos de Manganese: International Geology Congress 20th'', J.G. Reyna, ed. **5**, 221–272.

Cabella, R., Cortesogno, L., Gaggero, L. (1994): Hydrothermal contributions to cherts deposition in Northern Apennines: a preliminar report. *Ofioliti*, **19**, 367–376.

Cabella R., Lucchetti G., Marescotti P. (1998): Mn ores from Eastern Liguria ophiolitic sequences (''Diapri di Monte Alpe Formation'' Northern Apennines, Italy). *Trends Mineral*., **2**, 1–17.

Carignan, J., Hild, P., Mevelle, G., Morel, J., Yeghicheyan, D. (2001): Routine analyses of trace elements in geological samples using flow injection and low pressure on-line liquid chromatography coupled to ICP-MS: A study of geochemical reference materials BR, DR-N, UB-N, AN-G and GH. *Geostand. Newslett*., **25**, 187–198.

Cartwright, I. & Barnicoat, A.C. (1999): Stable isotope geochemistry of Alpine ophiolites: a window to ocean-floor hydrothermal alteration and constraints on fluid-rock interaction during high-pressure metamorphism. *Int. J. Earth Sci*., **88**, 219–235.

Castello, P. (1982): Il giacimento di Praborna (S. Marcel-AO). *Riv. Mineral. Ital*., **3**, 87–92.

Cenki-Tok, B. & Chopin, C. (2006): Coexisting calderite and spessartine garnets in eclogite-facies metacherts of the Western Alps. *Mineral. Petrol*., **88**, 47–68.

Cenki-Tok, B., Ragu, A., Armbruster, T., Chopin, C., Medenbach, O. (2006): New Mn- and rare-earth-rich epidote-group minerals in metacherts: manganiandrosite-(Ce) and vanadoandrosite-(Ce). *Eur. J. Mineral*., **18**, 569–582.

Ciriotti, M.E., Fascio, L., Pasero, M. (2009): Italian type minerals. Edizioni Plus, Pisa, 352 p.

Clauer, N., Stille, P., Bonnott-Courtois, C., Moore, W.S. (1984): Nd–Sr isotopic and REE constraints on the genesis of hydrothermal manganese crusts in the Galapagos. *Nature*, **311**, 743–745.

Compagnoni, R., Dal Piaz, G.V., Hunziker, J.C., Gosso, G., Lombardo, B., Williams, P. (1977): The Sesia-Lanzo Zone, a slice of continental crust with Alpine high pressure-low temperature assemblages in the Western Italian Alps. *Rend. Soc. Ital. Mineral. Petrol*., **33**, 281–334.

Constantinou, G. & Govett, G.J.S. (1972): Geology, geochemistry and genesis of Cyprus sulfide deposits. *Econ. Geol*., **68**, 843–858.

Cortesogno, L., Lucchetti, G., Penco, A.M. (1979): Le mineralizzazioni a manganese nei diaspri delle ofioliti liguri: mineralogia e genesi. *Rend. Soc. Ital. Mineral. Petrol*. **35**, 151–197.

Cronan, D.S. (1980): Underwater minerals. Academic Press, London, 362 p.

Dal Piaz, G.V. (1965): La formazione mesozoica dei calcescisti con pietre verdi fra la Valsesia e la Valtournanche ed i suoi rapporti strutturali con il ricoprimento del Monte Rosa e con la Zona Sesia-Lanzo. *Boll. Soc. Geol. Ital*., **84**, 67–104.

Dal Piaz, G.V. (1974): Le métamorphisme alpin de haute pression et basse température dans l'évolution structurale du bassin ophiolitique alpino-apenninique. *Boll. Soc. Geol. Ital*., **93**, 437–468; *Schweiz. Mineral. Petrogr. Mitt*., **54**, 399–424.

Dal Piaz, G.V. (2001): History of tectonic interpretations of the Alps. *J. Geodyn*., **32**, 99–114.

Dal Piaz, G.V. & Omenetto, P. (1978): Brevi note su alcune mineralizzazioni della falda piemontese in Valle d'Aosta. *Ofioliti*, **3**, 161–176.

Dal Piaz, G.V., Di Battistini, G., Kienast, J.-R., Venturelli G. (1979): Manganiferous quartzitic schists of the Piemonte ophiolite nappe in the Valsesia-Valtournanche area (Italian western Alps). *Mem. Sci. Geol*., **32**, 1–24.

Dal Piaz, G.V., Cortiana, G., Del Moro, A., Martin, S., Pennacchioni, G., Tartarotti, P. (2001): Tertiary age and paleostructural inferences of the eclogitic imprint in the Austroalpine outliers and Zermatt-Saas ophiolite Western Alps. *Int. J. Earth Sci*., **90**, 668–684.

Dasgupta, S. (1997): *P–T–X* relationships during metamorphism of manganese-rich sediments: Current status and future studies. *Geol. Soc. Spec. Publ*., **119**, 327–337.

De Negri, G. & Rivalenti, G. (1971): Alcune considerazioni sulla genesi dei giacimenti manganesiferi della Val Graveglia (Liguria). *Atti Soc. To. Sci. Nat. Mem, Ser. A*, **78**, 420–437.

de Saussure, H.-B. (1779–1796): Voyages dans les Alpes, précédés d'un essai sur l'histoire naturelle des environs de Genève. *S. Fauche, Neuchâtel*, **4**, 454–460.

Everitt, B.S., Landau, S., Leese M. (2001): Cluster analysis. 4th Edition, Wiley, New York, 259 p.

Fleet, A.J. (1983): Hydrothermal and hydrogenous ferromanganese deposits: Do they form a continuum? The rare earth element evidence. *in* ''Hydrothermal processes at seafloor spreading centers'', P.A. Rona, K. Bostrom, L. Loubier, K.L. Smith, eds. NATO Conference series, Plenum, New York, **12**, 535–555.

Frey, F.A., Bryan, W.B., Thompson, G. (1974): Atlantic ocean floor: geochemistry and petrology of basalts from Leg 2 and 3 of the Deep Drilling Sea Project. *J. Geophys. Res*., **79**, 5507–5527.

Glasby, G.P. (1978): Deep-sea manganese nodules in the stratigraphic records: evidence from DSDP cores. *Marine Geol*., **28**, 51–64.

Griffin, W.L. & Mottana, A. (1982): Crystal chemistry of clinopyroxenes from the St. Marcel manganese deposit, Val d'Aosta, Italy. *Am. Mineral*., **67**, 568–586.

Hein, J.R., Morgenson, L.A., Clague, D.A., Koski, R.A. (1987): Cobalt-rich ferromanganese crusts from the exclusive economic zone of the United States and nodules from the oceanic pacific. *in* ''Geology and resources potential of the continental margin of western North America and adjacent ocean basins'', D.W. Scholl, A. Grantz, J.G. Vedderm, eds. Circum-Pacific Council for Energy and Mineral Resources, Houston, 753–771.

Kienast, J.-R. (1973): Sur l'existence de deux séries différentes au sein de l'ensemble ''schistes lustrés-ophiolites'' du Val d'Aoste; quelques arguments fondés sur l'étude des roches métamorphiques. *C. R. Acad. Sci. Paris (série D)*, **276**, 2621–2624.

Kienast, J.-R. & Martin, S. (1983): I pirosseni egirin-giadeitici del livello basale di Praborna, Alpi occidentali. *Ofioliti*, **8**, 245–260.

Li, Y.-H. & Schoonmaker, J.E. (2003): Chemical composition and mineralogy of marine sediments. *Treatise Geochem*., **7**, 1–35.

Liou, J.G., Tsujimori, T., Zhang, R.Y., Katayama, I., Maruyama, S. (2004): Global UHP metamorphism and continental subduction/collision: the Himalayan model. *Int. Geol. Rev*., **46**, 1–27.

Manheim, F.T. (1978): Marine manganese deposits. Elsevier, Amsterdam, 523 p.

Marescotti, P. (1997): Studio delle mineralizzazioni a manganese associate a Diaspri di M. Alpe: mineralogia, composizione chimica, equilibri tra le fasi e significato genetico. Unpublished PhD thesis, Università di Genova, 93 p.

Marescotti, P. & Cabella, R. (1996): Significance of chemical variations in a chert sequence of the ''Diaspri di Monte Alpe'' Formation (Val Graveglia, Northern Apennine, Italy). *Ofioliti*, **21**, 139–144.

Martin, S. & Cortiana, G. (2001): Influence of the whole-rock composition on the crystallization of sodic amphiboles (Piedmont zone, western Alps). *Ofioliti*, **26**, 445–456.

Martin, S. & Kienast, J.-R. (1987): The HP–LT manganesiferous quartzites of Praborna, Piedmont ophiolite nappe, Italian western Alps. *Schweiz. Mineral. Petrogr. Mitt*., **67**, 229–360.

Martin, S. & Tartarotti, P. (1989): Polyphase HP metamorphism in the ophiolitic glaucophanites of the lower St. Marcel valley (Aosta, Italy). *Ofioliti*, **14**, 135–156.

Martin, S., Godard, G., Rebay, G. (2004): Walking on a palaeo ocean floor. The subducted Tethys in the Western Alps – an excursion guide. *in* ''Evolution of the western Alps: insights from metamorphism, structural geology, tectonics and geochronology'', M. Beltrando, G. Lister, J. Ganne, A. Boullier, eds. *J. Virtual. Explor*. (Electronic Edition), **16**, Paper 3.

Martin, S., Rebay, G., Kienast, J.R., Mevel, C. (2008): An eclogitised oceanic palaeo-hydrothermal field from the St. Marcel Valley (Italian Western Alps). *Ofioliti*, **33**, 49–63.

Martin-Vernizzi, S. (1982): La mine de Praborna (Val d'Aoste, Italie): une série manganésifère métamorphisée dans le facies éclogite. Unpublished PhD thesis, Université Pierre et Marie Curie (Paris), 215 p.

Millosevich, F. (1906): Sopra alcuni minerali di Val d'Aosta. *Riv. Min. Crist. It*., **33**, 34–40; *Rend. R. Acc. Lincei*, **15**, 317–321.

Mottana, A. (1986): Blueschist-facies metamorphism of manganiferous cherts: a review of the alpine occurrences. *Geol. Soc. Am. Mem*., **164**, 267–299.

Mottana, A. & Griffin, W.L. (1979): Pink titanite (greenovite) from St. Marcel, Valle d'Aosta, Italy. *Rend. Soc. Ital. Mineral. Petrol*., **35**, 135–143.

Mottana, A. & Griffin, W.L. (1982): The crystal chemistry of piemontite from the type-locality (St. Marcel, Val d'Aosta, Italy). *Reports 13th IMA Meeting*, 635–640.

Mozgawa, J. (1988): Comportement des éléments majeurs et traces au cours du métamorphisme éclogitique d'une série océanique manganésifère (mine de Praborna, Val d'Aoste). Unpublished PhD thesis, Université Pierre et Marie Curie (Paris), 142 p.

Murray, J. & Renard, A.F. (1891): Deep sea deposits. *Rep. Sci. Res. Exp. Voyage Challenger*, 525 p.

Nath, B.N., Plüger, W.L., Roelandts, I. (1997): Geochemical constraints on the hydrothermal origin of ferromanganese encrustations from the Rodriguez Triple Junction, Indian Ocean. *in* ''Manganese mineralisation: geochemistry and mineralogy of terrestrial and marine deposits'', K. Nicholson, J.R. Hein, B. Bühn, S. Dasgupta, eds. *Geol. Soc. Spec. Publ*., **119**, 199–211.

Perseil, E.A. (1988): La présence de strontium dans les oxydes manganésifères du gisement de St. Marcel-Praborna (Val d'Aoste, Italie). *Mineralium Deposita*, **23**, 306–308.

Perseil, E.A. (1998): Evolution cristallochimique des oxydes de manganèse dans le gisement de St. Marcel-Praborna (Val d'Aoste, Italie). *Rend. Lincei Sci. Fis. Nat*., **9/9**, 315–336.

Perseil, E.A. & Smith, D.C. (1995): Sb-rich titanite in the manganese concentrations at St. Marcel-Praborna, Aosta Valley, Italy: petrography and crystal-chemistry. *Mineral. Mag*., **59**, 717–734.

Perseil, E.A., Blanc, P., Ohnenstetter, D. (2000): As-bearing fluorapatite in manganiferous deposits from St. Marcel-Praborna, Val d'Aosta, Italy. *Can. Mineral*., **38**, 101–117.

Reinecke, T. (1985): Geochemistry of ferromanganoan metasediments from the island of Andros, Cycladic blueschist belt, Greece. *Chem. Geol*., **53**, 249–278.

Roy, S. (1981): Manganese deposits. Academic Press, London, 458 p.

Rubatto, D., Gebauer, D., Fanning, M. (1998): Jurassic formation and Eocene subduction of the Zermatt-Saas-See ophiolites: implications for the geodynamic evolution of the Central and Western Alps. *Contrib. Mineral. Petrol*., **132**, 269–287.

Smith, D.C. & Perseil, E.A. (1997): Sb-rich rutile in the manganese concentrations at St. Marcel-Praborna, Aosta Valley, Italy: petrography and crystal-chemistry. *Mineral. Mag*., **61**, 655–669.

Toth, J.R. (1980): Deposition of submarine crusts rich in manganese and iron. *Geol. Soc. Am. Bull*., **91**, 44–54.

Tumiati, S. (2005): Geochemistry, mineralogy and petrology of the eclogitized manganese deposit of Praborna (Valle d'Aosta, Western Italian Alps). Unpublished PhD thesis, Università dell'Insubria (Como)–Université Denis Diderot (Paris-7), 241 p.

Usui, A. & Someya, M. (1997): Distribution and composition of marine hydrogenetic and hydrothermal manganese deposits in the northwest Pacific. *in* ''Manganese mineralization: geochemistry and mineralogy of terrestrial and marine deposits'', K. Nicholson, J.R. Hein, B. Bühn, S. Dasgupta, eds. *Geol. Soc. Spec. Publ*., **119**, 177–198.

Usui, A. & Ito, T. (1994): Fossil manganese deposits buried within DSDP/ODP cores. Legs 1–126. *Mar. Geol*., **119**, 111–136.

Usui, A., Mellin, T.A., Nohara, M., Yuasa, M. (1989): Structural stability of marine 10 manganates from the Ogasawara (Bonin) Arc: implication for low-temperature hydrothermal activity. *Mar. Geol*., **86**, 41–56.

Received 22 September 2009
Modified version received 3 February 2010
Accepted 6 April 2010